Material Science and Technology Division

Propulsion Materials Program
Quarterly Progress Report for
April through June 2012

Allen Haynes
Technical Project Manager

Prepared for
U.S. Department of Energy
Assistant Secretary for Energy Efficiency and Renewable Energy
Office of Vehicle Technologies Program
VT 05 04 000

Prepared by the
OAK RIDGE NATIONAL LABORATORY
Oak Ridge, Tennessee 37831-6066
Managed by
UT-Battelle, LLC
for the Department of Energy
Under contract DE-AC05-00OR22725

CONTENTS

Project 18516 – Materials for Hybrid and Electric Drive Systems

Agreement 19201 – MBD Non-Rare Earth Magnetic Materials *(ORNL)*

Agreement 23278 - Low-Cost Direct Bonded Aluminum (DBA) Substrates *(ORNL)*

Agreement 23279 - Improved Organics for Power Electronics and Electric Motors *(ORNL)*

Project 18518 – Materials for High Efficiency Engines

Agreement 19202 – Titanium Friction and Wear *(ORNL)*

Agreement 23284 – Friction Reduction Through Surface Modification *(ORNL)*

Agreement 11752 – Materials for High Efficiency Engines *(ORNL)*

Agreement 13329 – Mechanical Reliability of Piezo-Stack Actuators *(ORNL)*

Agreement 17257 – Materials for Advanced Turbocharger Design *(ORNL)*

Agreement 18570 – Engine Materials Compatibility with Alternate Fuels *(ORNL)*

Agreement 18571 – Materials Issues Associated with EGR Systems *(ORNL)*

Project 18519 – Materials for Exhaust and Energy Recovery

Agreement 9130 – Catalyst Characterization *(ORNL)**

Agreement 10461 – Durability of Diesel Engine Particulate Filters *(ORNL)*

Agreement 10635 – Catalysts via First Principles *(ORNL)*

Agreement 19214 – Effects of Biodiesel Fuel on Diesel Particulate Filter Materials *(ORNL)*

Agreement 20091 – Electrically Assisted DPF Material *(ORNL)*

<u>Project 18865 – Application Specific Materials Simulation, Characterization and Synthesis</u>

Agreement 9105 – Characterization of Catalyst Microstructures *(ORNL)*

Agreement 14957 – High Temperature Thermoelectrics *(ORNL)*

Agreement 16308 – MBD Thermoelectrics Theory and Structure *(ORNL)*

_____

***No report this period.**

Agreement 19201: Non-Rare Earth Magnetic Materials

Michael A. McGuire
Oak Ridge National Laboratory

Objective/Scope

We will examine rare-earth-free chemical systems which hold promise for the discovery of new high-temperature ferromagnets with the large magnetic moments and strong anisotropies required for technologically useful permanent magnet materials. This research will focus on the development of new rare-earth free permanent magnet materials. Understudied chemical systems which are likely to contain materials with properties required for useful ferromagnets (large moments, high Curie temperatures, strong magnetic anisotropy) will be synthesized and characterized. First principle calculations will be performed to aid in the identification of promising target materials and to guide chemical tuning of magnetic properties through element substitutions and alloying. The focus will be on materials based on elements, such as Mn, Fe, Co and Cr, suitable for application in vehicles.

The primary challenge in this work is to obtain high magnetic anisotropy without rare-earth elements, while maintaining high saturation magnetization. The two main sources of anisotropy are magneto-crystalline anisotropy and shape anisotropy. Magneto-crystalline anisotropy is an intrinsic property determined by energy required to rotate a magnetic moment relative to the crystal lattice. Shape anisotropy is an extrinsic property related to the domain structure of individual crystallites. We are targeting intermetallic compounds with large magneto-crystalline anisotropy, which could then be further enhanced by materials processing to optimize magnetic domain configurations. To obtain anisotropic magnetic properties, heavy transition metal elements will be incorporated instead of rare earths.

Technical Highlights

Two technical reports were published in the open scientific literature this quarter. See references below in “Publications/Presentation/Awards”.

The first summarized our discovery and investigation of the new ferromagnets $ZrFe_{12-x}Al_x$ and $HfFe_{12-x}Al_x$. This combined experimental and theoretical work has been highlighted in a previous quarterly report.

The second concerns the complex ferromagnet $Cr_{11}Ge_{19}$. Work on this compound was led by UT Knoxville Physics graduate student Nirmal Ghimire. This material has a very anisotropic crystal structure. It is tetragonal with a c/a ratio of ~9 (a = 5.8 Å, c = 52.3 Å). The Curie temperature is low (88 K) and the remanent magnetization is small; however, study of this material produced good science and highlights some interesting physics associated with low-symmetry ferromagnetism. In addition to being strongly uniaxial, the crystal structure of $Cr_{11}Ge_{19}$also lacks an inversion center. The lack of inversion symmetry in a ferromagnetic material allows some unusual and complex magnetic interactions to take place. Often this results in what is known as helimagnetism. The

magnetic moments are not collinear in the ordered state, but instead their directions follow a helix that propagates along a specific crystallographic direction. These helices can interact in peculiar ways with each other and with an external magnetic field. Complex behaviors suggesting such interactions may indeed be important in $Cr_{11}Ge_{19}$ were observed in both experimental data and first principles. In addition, we reported evidence of strong magneto-elastic effects, causing an unusual response of the crystal lattice and its vibrations to the onset of magnetic ordering.

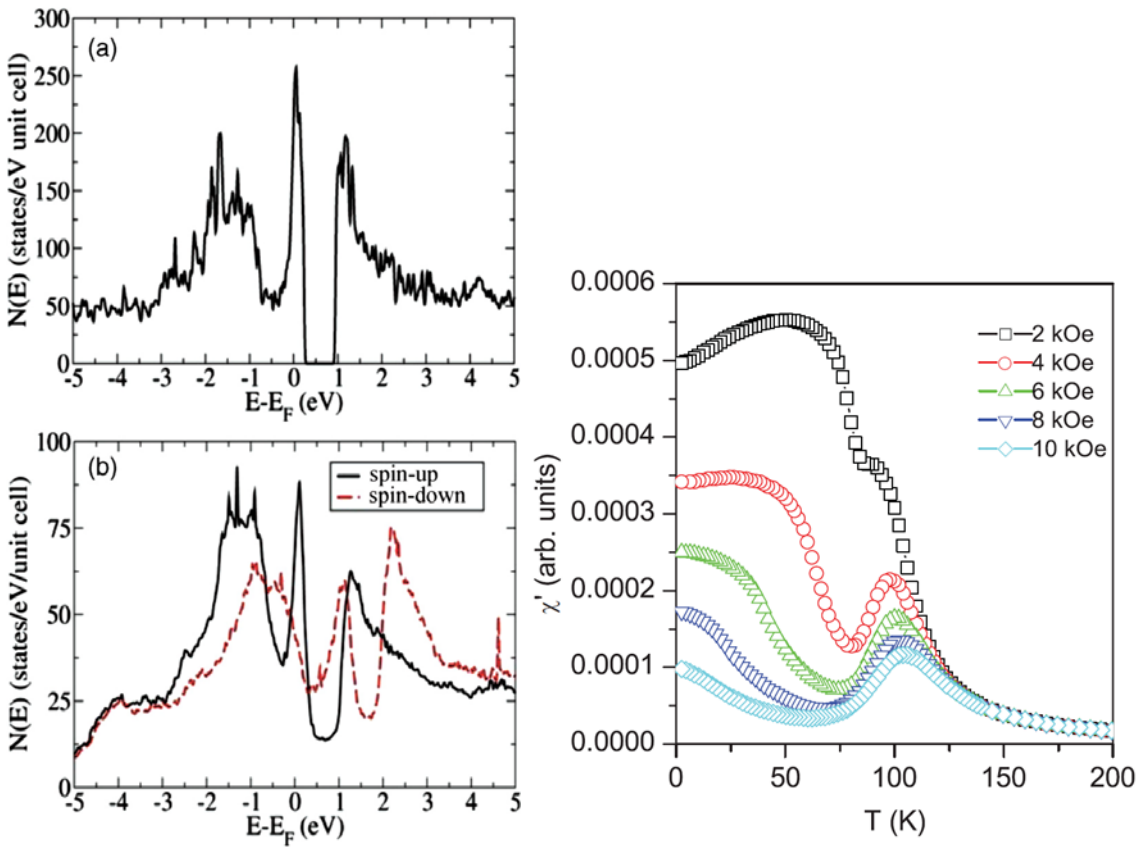

Figure 1. (left) Calculated electronic structure of $Cr_{11}Ge_{19}$ in the non-magnetic state (a) and ferromagnetic state (b), supporting itinerant ferromagnetism in this compound. (right) The measured AC magnetic susceptibility of $Cr_{11}Ge_{19}$. The unusual behavior reveals similarities to known helimagnetic materials.

Status of FY 2012 Milestones

(1) Determine usefulness of metal flux synthesis technique for producing crystals of new ternary phosphides with transition metal concentrations approaching and exceeding 70 %, anisotropic structures, and Curie temperatures in excess of 300 °C. Results will be summarized in a report and, if appropriate, a manuscript for publication in the scientific literature. (09/2012)

Specific ternary compounds (primarily phosphides) are being targeted in parallel using this approach and more traditional powder-metallurgy techniques. Solubility of refractory metals and iron continues to present challenges.

(2) Develop capabilities to produce sub-nitrides using flowing ammonia gas, and examine effects of mild nitriding conditions on magnetic intermetallic compounds, with the aim of enhancing Curie temperature to values above 300 °C and increasing their magnetic anisotropy, a requirement to produce energy products competitive with RE magnets (~ 30 MG Oe). Results will be summarized in a report and, if appropriate, a manuscript for publication in the scientific literature. (09/2012)

Arrangements have been made to conduct nitriding experiments in the Materials Chemistry Group in the Chemistry Division at ORNL. These facilities will be used by the project for the remainder of FY2012. Starting alloys to be used for the next round of nitriding experiments have been synthesized.

Communications/Visits/Travel

None to report.

Problems Encountered

None to report.

Publications/Presentations/Awards

M.A. McGuire, N. Ghimire, D.J. Singh, "Ferromagnetism in $ZrFe_{12-x}Al_x$ and $HfFe_{12-x}Al_x$ (x = 6.0, 6.5, 7.0)" Journal of Applied Physics **111** (2012) 093918.
DOI: 10.1063/1.4712445

N.J Ghimire, M.A. McGuire, D.S. Parker, B.C. Sales, J.Q. Yan, V. Keppens, M. Koehler, R.M. Latture, D. Mandrus, "Complex itinerant ferromagnetism in noncentrosymmetric $Cr_{11}Ge_{19}$" Physical Review B **85** (2012) 224405. DOI: 10.1103/PhysRevB.85.224405

References

None.

Agreement 23278: Low-Cost Direct Bonded Aluminum (DBA) Substrates

H. -T. Lin, A. A. Wereszczak, and Shirley Waters
Oak Ridge National Laboratory

Objective/Scope

This project seeks to develop low-cost, high quality, and thermomechanically robust direct-bonded aluminum (DBA) substrates. Low-cost DBA substrates will lessen the cost of the inverter insulated gate bipolar transistor (IGBT) power modules while concomitantly sustaining or improving thermal management and improving thermomechanical reliability. Compared to copper and DBC substrates, aluminum has a lower elastic modulus so it imparts a lower stress on the ceramic substrate it sandwiches, and this contributes to improved mechanical reliability of the entire substrate. Wire and ribbon for bonding in power electronic modules tends to be aluminum, so the apparent coefficient of thermal expansion of DBAs is compatible with them unlike DBCs. The use of a DBA substrate will also lessen the weight up to 50% compared to presently used DBC substrates, and this would contribute to the weight reduction goals of the inverter and converter in the APEEM program as well.

Technical Highlights

Microstructure of a developmental Cu-cladding Al ribbon was analyzed via scanning electron microscopy (SEM) equipped with a EDAX system, as shown in Figure 1. The advantages of application of Cu-cladding Al ribbon are the Cu-cladding Al material exhibits 45% higher thermal conductivity and also could carry 30% higher current density than Al substrate alone. Also, the analysis showed that the Al material used in this Cu-cladding ribbon is a Si-rich Al alloy (Fig. 1), which might be directly bonded to ceramic substrates without the use of brazing materials. Initial attempts were made to bond the Cu-cladding ribbon to AlN and Al_2O_3 ceramic substrate at temperature ranging between 580 and 600°C for 30 minutes under an applied load of 5 MPa in Ar. All results showed that there did not exhibited any bonding between the ribbon and ceramic substrates even there was an evidence that the temperatures employed reached the eutectic point of Si-rich Al alloy. Figure 2 showed the microstructure of Si-rich Al layer after the hot pressuring at high temperature. The composition analysis via EDAX showed that the eutectic phases observed were Cu-Al alloys, but not the Al-Si composition. Note the Cu and Al alloy exhibited a eutectic point at 548°C, which is lower than the Al-Si eutectic point of 577°C. The formation of Al-Cu eutectic phases might occur much earlier than the Al-Si eutectic phase during the processing, resulting in no reaction and thus no boding between the Si-rich Al layer and ceramic substrates. An alternative bonding approach needs to be searched and devised to ensure a strong bonding between Cu-cladding Al ribbon and ceramic substrates.

Direct-bonded aluminum (DBA) substrates fabricated with AlN could exhibit piezoelectric response under a combined of high electric field and external applied load. A preliminary investigation of piezoelectric response for a commercial DBA was conducted during this reporting period. The piezodiatometer was used to test the DBA under the applied voltage of 1252 and 1878 peak voltage that corresponded to 2 and

3 kV/mm, respectively. The measured displacement output indicated that there was no piezoelectric response under the test conditions employed. This could be attributed the fact that the AlN has very low piezoelectric coefficients (d33 ~ 5 pm/V, d31 ~ -2 pm/V). Alternative approaches with the much higher applied electric field and/or externally applied load might be needed to characterize the piezoelectric property.

As stated in previous report that the electronic substrates with silicon nitride ceramic substrate have been developed and commercialized for the higher temperature and voltage application conditions due to its much better mechanical performance (fracture strength and toughness) compared to Al_2O_3 and AlN. Thus, study to characterize the thermal conductivity of silicon nitride ceramics developed at ORNL with both high fracture toughness (up to 12 MPa•$m^{0.5}$) and strength (up to 1200 MPa) was initiated. The thermal conductivity was measured using a laser flash technique. The preliminary results showed that the silicon nitride sintered with 8% Gd_2O_3 and 2% SiO_2 exhibited the thermal conductivity of 42.8 W/cm•K, and the one sintered with 8% Lu_2O_3 and 2% MgO exhibited the thermal conductivity of 77.6 W/cm•K. Note that the microstructure and composition of these ORNL silicon nitride ceramics were tailored for the purpose of high performance structural component applications, as shown in Figure 3. It is reasonable to anticipate that the thermal conductivity of these ORNL silicon nitride ceramics could be significantly improved via the careful engineering of microstructure and compositions.

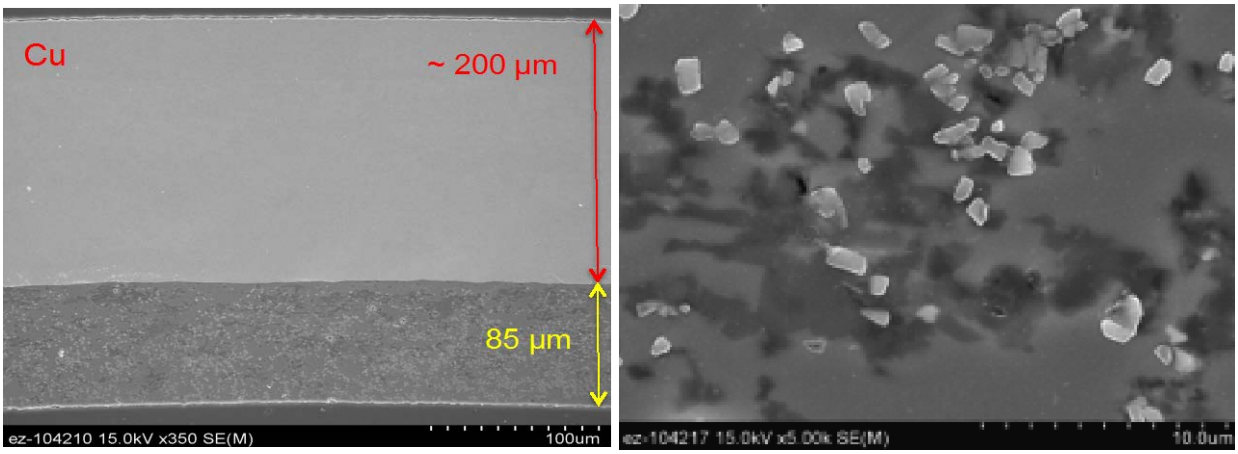

Figure 1. SEM micrograph of a SEM micrographs of an as-received developmental Cu-cladding Al ribbon.

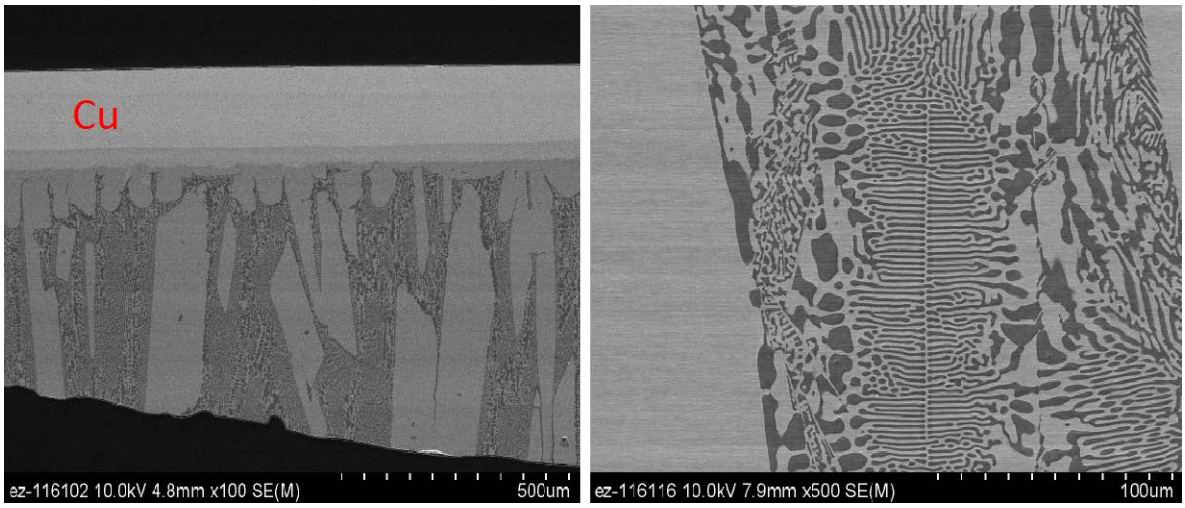

Figure 2. SEM micrographs of a developmental Cu-cladding Al ribbon after the bonding process at 600°C for 30 minutes. Note that the formation eutectic morphology of Al-Cu alloy was observed (RHS).

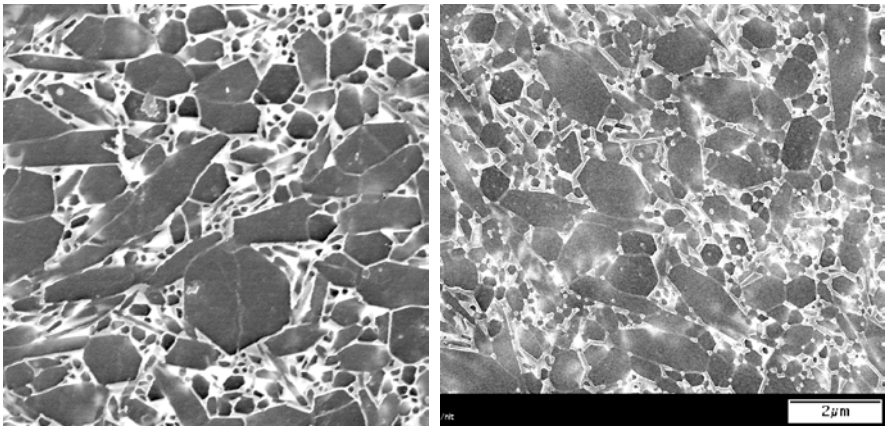

8%Lu_2O_3-2MgO 8%Gd_2O_3-2SiO_2

Figure 3. SEM micrographs of a ORNL silicon nitride with 8% Lu_2O_3 and 2% MgO and 8% Gd_2O_3 and 2% SiO_2 sintering additives.

<u>Status of FY 2012 Milestones</u>

(1) Complete characterization of microstructure, and physical (coefficient of thermal expansion and thermal conductivity) and mechanical strength of commercially available DBA substrates up to 200°C**. (09/2012)** – **On schedule**.

(2) Complete fabrication of DBA substrates manufactured via new ORNL processing method and compare thermal cycling response between –40°C and +150°C in air against that of commercial DBA substrates**. (09/2012) – Delayed**. The delay was due to the lake of adequate commercially available brazing pastes and thus the fabrication of DBA substrates with a adherent and strong bonding could not be realized.

Communications/Visits/Travel

- Several discussions have occurred with ORNL/NTRC, USCAR EETT, General Motors, and Delphi staff members about the research and benchmarking plans for this project.

Problems Encountered

The commercial Al-Si brazing paste employed could not provide adequate strong bonding between Al and ceramic substrates. Search for new brazing products would be needed to ensure an adherent and strong bonding.

Publications/Presentations/Awards

Oral presentation of this project was presented at DOE Annual Peer and Merit Review, Washington, D. C., May 14-17, 2012.

References

1. P. D. Desal, “Thermodynamic Properties of Selected Binary Aluminum Alloy Systems,” J. Phys. Chem. Ref. Data, Vol. 16, No. 1, 1987.
2. Y. Sakai and H. Ishiyama, “Power Control Unit for High Power Hybrid System,” 2007-01-0271, Advanced Hybrid Vehicle Powertrains, 2007 World Congress, SAE International, 2007.
3. T. Nishimura, Y. Takamiya, and O. Nakajima, “High Power IGBT Modules,” pp. 51-55, Fuji Electric Review, Vol. 55 [2], 2009.
4. Y. Zhou, H. Hyuga, D. Kusano, Y. Yoshizawa, and K. Hirao, “A Tough Silicon Nitride Ceramic with High Thermal Conductivity,” Adv. Mater. 2011, 23, 4563-4567.

Agreement 23279: Improved Organics for Power Electronics and Electric Motors

A. A. Wereszczak, T. G. Morrissey, and H. Wang
Oak Ridge National Laboratory

Objective/Scope

Identify lower-cost and better-performing organic compounds for dielectric and thermal management applications in power electronics and electric motors. Candidate and new organic compounds (e.g., epoxy molded compounds or EMCs) will be characterized and developed to promote low-cost fabrication, volume reduction, mechanical resilience, and improved and alternative thermal management exploitation. They include compounds presently used in dielectrics in power electronic devices, potting compounds used with capacitors, and pottings used in motors. For dielectrics, improved performance represents a higher-temperature capability and the sustainment of dielectric and gel-like mechanical damping properties under thermal cycling and vibratory conditions. For potting compounds used with capacitors or motors, interest exists to identify alternatives that have higher thermal conductivity (or that enhance the thermal conductivity of existing compounds) or that benefit structural or damping performance without compromising thermal performance.

Technical Highlights

The first group of magnesium-oxide- (MgO) filled epoxy molding compounds (EMCs) were received from SolEpoxy (Olean, NY). Ube provided the MgO powder. Four sets were produced by SolEpoxy. One was a baseline epoxy (no filler), and the other three sets contained MgO powder with different particle size distributions (PSDs) but the same amount of MgO in each (nominally 75 wt % or 49 vol %). One MgO PSD had a d50 of 10.9 µm and was used in one set. The other MgO PSD had a d50 of 62.7 µm and comprised a third set. The fourth set was a 50/50 blend of the two powders. The four sets are shown in Figure 1.

Various measured properties of the MgO-EMCs are shown in Table I. Apparent density was calculated by dividing the disk mass by its volume. The room temperature thermal conductivity was measured using a hot disk thermal constants analyzer. The elastic modulus and Poisson's ratio were determined using resonant ultrasound spectroscopy (RUS).

Being that the goal is to produce a thermally conductive, electrically insulative EMC, another processing set was initiated to increase the volume fraction of added powder. This set was received at the very end of Q3, and its properties will be measured. A thermal conductivity increase of 10x, over that of the unfilled epoxy, is sought but the results shown in Table I show just an 8x increase so far. The new set, with its higher volume fraction of filler, should satisfy that 10x increase objective. But future work will seek the achievement of 5 W/mK of a MgO-filled EMC (a 20x increase over the baseline epoxy). NTRC's John Miller, a PI on a VT PEEM Program project on motor development, indicated the achievement of 5 W/mK could significantly benefit motor thermal management. Thermal modeling previous done on this project also showed

that an EMC thermal conductivity of 5 W/mK would also enable new thermal management options for power electronic modules and film capacitors, too.

Figure 1. Disks of developmental MgO-filled MgO-EMCs

Table I. Property measurements of MgO-filled EMCs

Set	Density (g/cm^3)	Thermal Conductivity (W/mK)	Elastic Modulus (GPa)	Poisson's Ratio
Epoxy (unfilled)	1.19	0.24	3.0	0.32
MgO-EMC (66A)	2.35	2.35	19	0.28
MgO-EMC (66B)	2.36	2.21	18	0.27
MgO-EMC (66C)	2.42	2.00	20	0.25

Status of FY 2012 Milestones
Model, design, and fabricate filler-containing-EMC having 10x thermal conductivity increase over monolithic epoxy. [Sep12] *On schedule.*

Communications/Visits/Travel:
Numerous discussions were held with SolEpoxy's Robert Groele, Phil Farris, and Chuck Volante about ongoing MgO-filled EMC collaborative work. Discussions were held with NTRC's John Miller about the measured properties of these development MgO-EMCs.

Problems Encountered
None

Publications/Presentations/Awards
Wereszczak gave a presentation entitled "Improved Organics for Power Electronics and Electric Motors" at the 2012 Vehicle Technologies Annual Merit Review, Arlington, VA, on 15 May 2012.

References
None

Agreement 19202: Titanium Friction and Wear (Surface Engineering of Bearing Components)

Peter Blau
Oak Ridge National Laboratory

Objective/Scope

The energy efficiency of internal combustion engines (ICEs), whether fueled by conventional or alternative fuels, benefits from the use of lightweight materials. Examples include fiber-reinforced composites and alloys of aluminum, magnesium, and titanium. While such materials offer attractive efficiency gains, their use also presents technical and economic challenges. One class of ICE applications involves tribological aspects: that is, those which concern friction, wear, and lubrication. Studies in the United States, Japan, and the United Kingdom have shown that mechanical losses comprise about fifteen percent of the energy dissipation from fuel in a typical ICE, and that of those, energy losses by friction comprise about eighty percent. The two major subsystems, in terms of engine frictional losses, are the piston ring/cylinder interface and the crankshaft bearings, including those on the connecting rods. The current project which began in FY 2010 not only addresses the potential use of lightweight alloys in connecting rod bearings, but it also investigates the degree to which surface engineering and coating technologies could benefit other friction- and wear-critical applications.

The objective of this project is to *provide the diesel industry with surface technology options to enable lightweight titanium (Ti) alloys to be used for wear and friction-sensitive engine components like connecting rods (CRs) and crankshafts.* Its goal is to identify the most promising surface engineering methods, whether commercialized or experimental, that can reduce friction and wear of Ti alloys under lubricated, engine-like conditions. This work compliments recent developments in Ti technology that portend reduced alloy cost. The phases of this three-year effort that began in FY 2010 are: 1) *Friction and wear screening* of multiple surface treatments and coatings for titanium using ASTM standard coupon tests to down-select leading performers, 2) *Design and construction of a computer-controlled, variable load bearing tester* (VLBT) to simulate the contact pressure and lubricant regime excursions experienced by connecting rod bearings, and 3) Preparation of a realistic assessment of whether any of the *surface engineering methods evaluated in this project, be they commercially-available or experimental, could beneficially be applied to Ti alloys for use in diesel engine connecting rods and other rubbing parts that must last for as many as a million miles of service*.

Technical Highlights

During this quarter, the newly commissioned variable load bearing test (VLBT) system was used to evaluate surface treatments that passed friction and wear screening tests during earlier phases of the project. New results were obtained on the state of micro-strain underlying mechanical surface treatments like shot peening and planishing when applied to titanium alloy Ti-6Al-4V. Finally, the effects of applying spectrum load

profiles to test the friction of several surface treatments were determined, and work was begun on a final report.

X-ray Analysis of Ti-Alloys with Work-hardened Surfaces. A portion of this effort was devoted to characterizing the potential friction and wear benefits from synergistic effects of multiple surface treatments of Ti alloys. For example, shot peening has been used in conjunction with nitriding. In that case, mechanical working was performed after heat treatment because performing the heat treatment as a last step would diminish the effects of work hardening. Results of this study are being submitted to the *19th International Conference on Wear of Materials* (April 2013). Both bearing steel (AISI 52100) and silicon nitride (NBD 200) were used as sliders in reciprocating sliding tests to investigate the effects of adhesive transfer and differential hardness between the slider and its counterface. As part of the multiple treatments study, Dr. Melanie Kirkham, ORNL, conducted micro-strain x-ray studies of the surfaces of the Ti alloys. Their purpose was to correlate differences in the near-surface strain state, due to processing, with the wear and frictional performance. Diffraction patterns were collected with a PANalytical X'Pert Pro diffractometer in Bragg-Brentano geometry with Cu Kα radiation (λ = 1.5406 Å). The penetration depth (99%) into Ti-6-4 under those conditions is estimated to be 5-16 μm, depending on the angle of incidence. Figure 1 summarizes the results of that characterization.

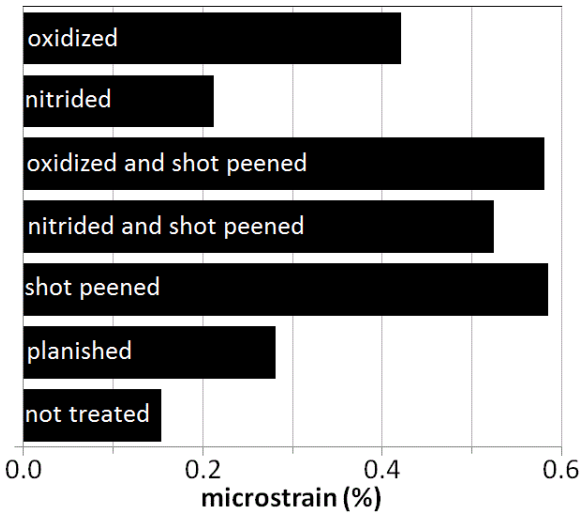

Figure 1. Microstrain results comparing various surface treatments applied to Ti alloy.

Shot peened surfaces had approximately four times the subsurface micro-strain than the non-treated Ti alloy, and thermal oxidation produced more subsurface micro-strain than did nitriding. Shot-peened Ti-6Al-4V surfaces had the highest microstrains after multiple surface treatments were applied. The not treated (bare) surface had the least microstrian, as would be expected. As is described in the conference paper, the main benefits of combined treatments seemed to be to delay a transition from mild wear to severe wear, as is experienced with non-treated Ti.

Spectrum Loading Tests of Surface Engineered Titanium. During the first year of this effort, over twenty candidate methods for improving the friction and wear of titanium surfaces were evaluated using ASTM G133, a standard test method for reciprocating ball on flat sliding wear. Procedure B of the standard was used with engine conditioned diesel oil as the lubricant. Results were presented previously [1]. As a result of the first year's work, several of the more promising candidates were down-selected for screening on a new, variable load bearing tester (VLBT) that was being designed and built during that time to simulate the changing load profiles experienced by a connecting rod large end bearing. The following two reference materials and five promising surface engineering candidates were tested in the second phase of this effort:

- Bare titanium (Ti-6Al-4V) alloy (as the baseline)
- Bronze alloy CDA 932 (typical bearing alloy for engine plain bearings)
- Oxygen diffusion treated (OD) Ti-6Al-4V
- Nitrided Ti-6Al-4V
- Commercial TiN sputter coated Ti-6Al-4V
- Commercial CrN coated Ti-6Al-4V
- Diamond like carbon

In addition, we decided to include two more materials for comparison.

- Commercial anodized Ti-6Al-4V coated with a filled polymer composite
- Carburized Ti-6Al-4V that 'failed' the first phase of screening.

The first additional material offered an opportunity that presented itself more recently, and the second material was included to see whether a material that failed on type of test, my provide successful under a different lubrication regime, as is present in the VLBT. It turned out that the diamond film wore through and showed evidence of cracking at the edge of the wear scar during initial screening, so it was not included in latest experiments.

VLBT tests were programmed to simulate the load variations during an operating large end connecting rod bearing. The spectrum was adopted from Taylor's analysis of engine bearings [2]. The load (P) versus time (t) for one cycle (see Figure 2) is from a baseline test on bronze.

Friction force versus friction coefficient data were compiled for duplicate runs on each material combination. It was noted that in most cases, the friction coefficients were quite low (< 0.05) which would put them into the mixed or nearly full-film lubrication regime. In contrast, friction coefficients measured in the previous ASTM G133 tests were generally higher, typical of the boundary lubrication regime. This is because the VLBT has a converging-wedge line contact that better simulates a plain bearing configuration. The G133 allows lubricant to flow around the reciprocating pin specimen and therefore cannot develop the kind of stable film that lowers friction. Friction results were compiled from the ten cycle of spectrum testing and the results indicated a range of values as the load varied during the cycle. Figure 3, for example compares the range of friction coefficients for the tenth load cycle of a series of candidate treatments

tested in the VLBT. While the nitride treatment had the lowest friction during one part of the load cycle, it had the highest friction during another part. The carburized treatment, which incidentally failed the tests performed with a different apparatus and test method, actually performed among the best under the different lubrication regime provided by the VLBT apparatus. Four of the treatments had considerably lower friction than the baseline bronze during a portion of the loading cycle.

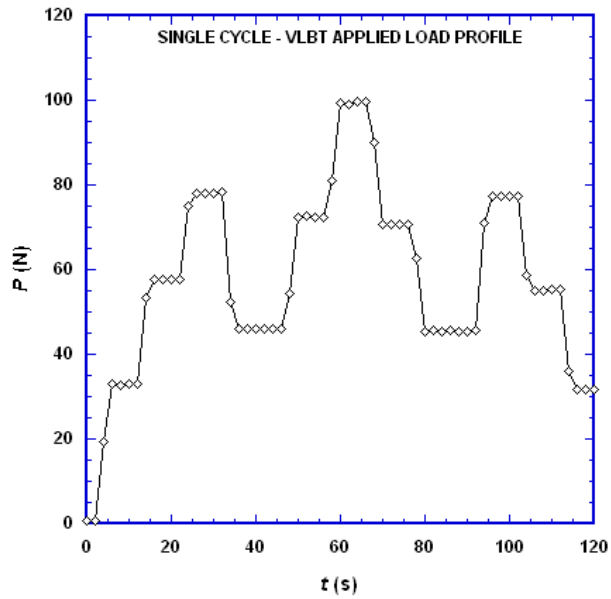

Figure 2. The load profile applied to the test specimens multiple times for a typical test of surface treatments. Each test ran 10 load cycles at 0.5 m/s sliding speed. Frictional running-in tended to occur within the first half-cycle on the majority of tests.

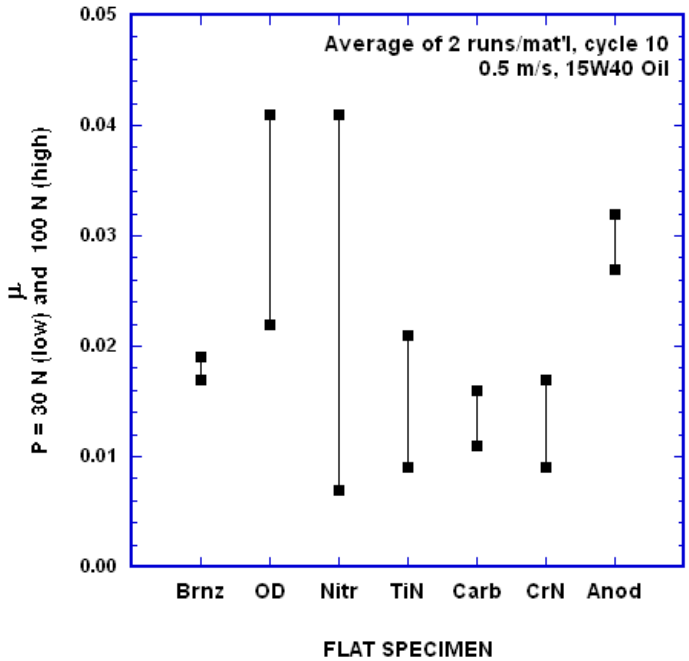

Figure 3. Range of friction observed during the 10th cycle of VLBT tests on carious surface treatments.

Finally, an informal collaboration has been established with Penn State University's Applied Research Laboratory (Prof. A. Segall) to conduct a few experiments on a novel coating process they developed, called high velocity particle consolidation ('cold-spray'). Several specimens of coated Ti-6Al-4V alloy coated at Penn State will be tested and the friction and wear behavior will be compared to the leading candidate treatments shown in Figure 3.

Future Plans

- Complete testing of the effects of spectrum loading on the friction and wear of surface engineered titanium, including to the extent time allows a few exploratory tests on a recently-developed Penn State University coating.
- Complete a draft of the final report that assessed the potential use of surface engineered titanium as a sliding bearing surface in a connecting rod large-end bearing and other sliding components in engines.

Status of Milestones

1) Complete tests of candidate coatings and multiple surface treatments using the variable-load bearing test system (VLBT)**. (09/11)** Postponed to work out apparatus design issues, but now completed as of 6/12.

2) Complete analysis of VLBT test surfaces and prepare a final report summarizing the work on this effort that culminates in a design concept for Ti-alloy connecting rods with integral bearing surfaces. **(09/12)** On schedule.

Communications/Visits/Travel

None this quarter

Problems Encountered

None

References

[1] D. G. Bansal, O. L. Eryilmaz, and P. J. Blau (2011) Surface engineering to improve the durability and lubricity of Ti-6Al-4V alloy," *Wear*, Vol. 271, 2006-2015.

[2] C. M. Taylor (1993) "Engine Bearings: Background and Lubrication Analysis," Chapter 5 in *Engine Tribology*, ed. C. M. Taylor, Elsevier Pub., The Netherlands, pp. 89-112.

Publications and Presentations

1) D. G. Bansal, M. Kirkham, and P. J. Blau, "Effects of combined diffusion treatments and cold working on the sliding friction and wear behavior of Ti-6Al-4V," abstract accepted for the *19th International Conference on Wear of Materials*, Portland, OR. 14-18 April 2013, both as an oral presentation and as a journal article for the proceedings.

2) P. J. Blau[1], K. M. Cooley, and D. Bansal**, "**Spectrum loading effects on the running-in of lubricated bronze and surface-treated titanium against alloy steel," abstract accepted for the *19th International Conference on Wear of Materials*, Portland, OR. 14-18 April 2013, both as an oral presentation and as a journal article for the proceedings.

Agreement 23284: Friction Reduction Through Surface Modification

Peter J. Blau
Oak Ridge National Laboratory
and
Stephen M. Hsu
George Washington University

Objective/Scope

The objective of this two-year effort is to improve the fuel efficiency of diesel-powered vehicles by employing carefully designed patterns of micro-scale features to reduce the friction of relatively-moving, load-bearing surfaces. These textures function in two ways: (1) by increasing the thickness of the lubricant film in order to separate bearing surfaces, and (2) by trapping harmful wear debris particles in depressions below the contact surface. One bearing surface of particular interest is that between the piston ring and cylinder liner, although other frictional surfaces in engines, like those of bucket lifters and cam lobes are also of interest.

The scope of this effort includes the preparation and testing of textured metallic surfaces produced by various surface engineering methods. During FY 2011, ORNL prepared indentation-textured surfaces on bearing materials, and investigated the effects of on wear and friction as a function of sliding time. Changes in the morphology of the surfaces during the running-in stages were correlated with the friction coefficient versus time sliding history. Understanding the running-in period is key to separating the contributions of as-finished surface roughness, wear-in, and lubricant conditioning as the bearing system approaches its longer-term, steady-state condition. A subcontract with George Washington University complements in-house efforts by developing and demonstrating a new masking technology to enable the surface patterning of curved surfaces like those on piston rings and cylinder bores.

Technical Highlights

Compression texturing produces friction reduction. Experiments continued on the effects of compression texturing (CTx) on the friction of bearing surfaces using CDA 932 leaded bronze as the model plain bearing material. The ORNL variable load bearing tester (VLBT) uses a flat (bronze) specimen loaded upward against a spinning cylinder of 8620 alloy steel (sliding speed 0.1 m/s) under drip lubrication by 15W40 diesel oil. It was programmed to apply a sequence of loads patterned after the typical force versus crank angle behavior of an internal combustion engine's connecting rod large end bearing. A load profile from a typical VLBT test is shown in Figure 1. Note that the load varies between 32 and 100 N in a series of steps, and one full cycle takes 120 seconds.

The friction coefficients and wear features for flat, 6 µm diamond-polished bronze specimens was compared to that for a CTx surface that was initially polished to a 6 µm diamond finish and then impressed, using a servo-hydraulic compression testing machine, with two different square grids of high modulus woven wire (20x20/inch, 50x50/inch). For the fine grid, a final polishing step was added to remove the ridges

that formed as a result of indenting with the mesh. Ten 120-second load cycles were applied in each test. The first cycle was intended to run-in the surface, and the last (10th) cycle was used for friction measurements typical of steady-state.

Friction coefficients were digitally sampled and averaged over 2 second intervals. In keeping with the Stribeck relationship shown in Figure 2 and explained in prior reports, the inverse of the applied load (*P*) during the last (10th) cycle of each test was plotted versus the corresponding friction coefficient.

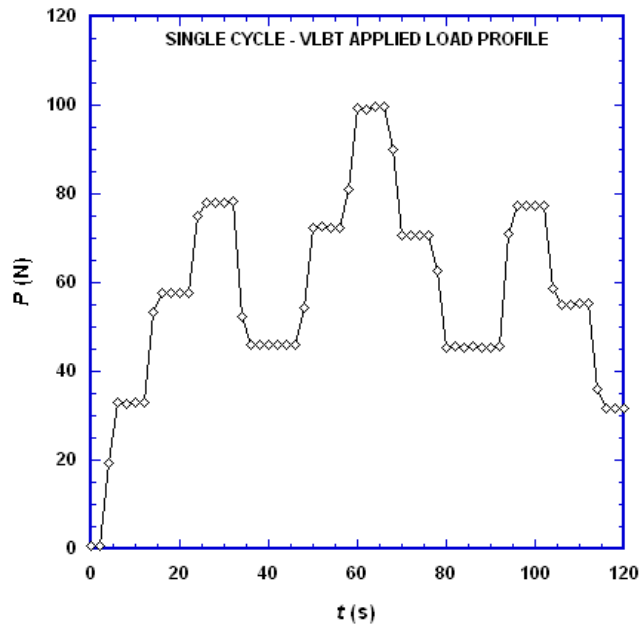

Figure 1. Load versus time (single cycle) that simulates a connecting rod bearing.

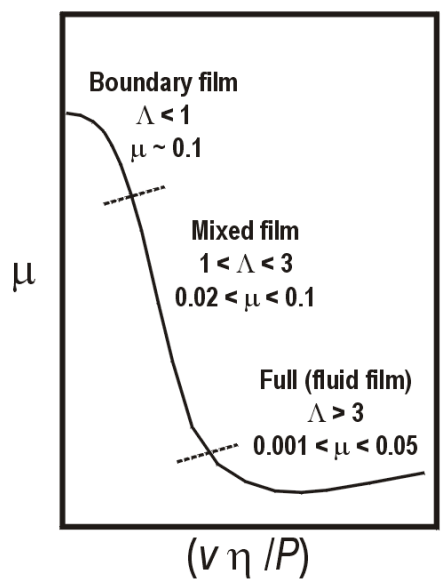

Figure 2. Stribeck relationship for sliding lubricated friction as a function of velocity (v), viscosity (η), and load (P).

Results from the experiments on polished, coarse grid CTx, and fine grid CTx specimens are shown in Figure 3. These compare the friction versus load response for the 10th cycle of each test. Compared with Figure 2, the plot in Figure 3 represents the lower area of the Stribeck curve in which there is a transition between mixed and full-film lubrication. Coefficients for a second-degree polynominal fit for the data, shown at the top of the figure, are for the relationship:

$$\mu = \mathrm{Mo} + \mathrm{M1}\ (1/P) + \mathrm{M2}\ (1/P)^2 \qquad (1)$$

The presence of coarse grooves in the surface shifted the Stribeck curve upward to higher friction values, but the fine-textured surface, followed by polishing to remove the rims, produced a 50% reduction in friction.

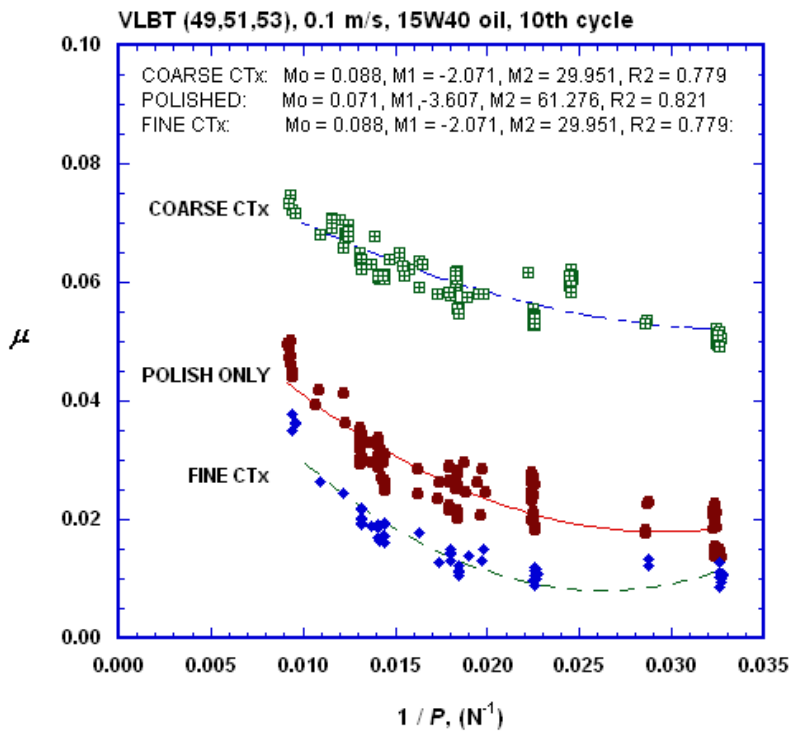

Figure 3. Friction coefficient (μ) plotted against inverse applied load from the 10th cycle of VLBT tests for polished, coarse-textured, and fine-textured bronze. Coarse texture increased the friction but fine texture reduced it.

In a recent review of surface patterning methods for friction reduction [1], it was noted that due to the many possible attributes of textured surfaces, not every design results in frictional benefits, and the current case amply shows that effect. One reason for the rise in frictional behavior of coarse CTx can be seen in part in Figures 4(a) and (b) which compare the wear markings on two of the test specimens. Clearly, solid-solid contact and wear occurred, and it cannot be claimed that full film lubrication (that is, complete surface separation) existed during these tests despite the low friction coefficients and the shape of the (1/*P*) versus μ curve. Furthermore, we note that the

scuffing along the patterned grooves in Figure 4(b) suggests that there were upstanding ridges around the compressed pattern that prevented full contact. Had there been fuller contact – as in the finer grid – the wear scar would have looked more like the abrasive markings seem in Figures 4(a) or 5, and the friction would probably have been lower. Encouraging results from the fine-textured, post-polished surface will be further explored in the upcoming quarter.

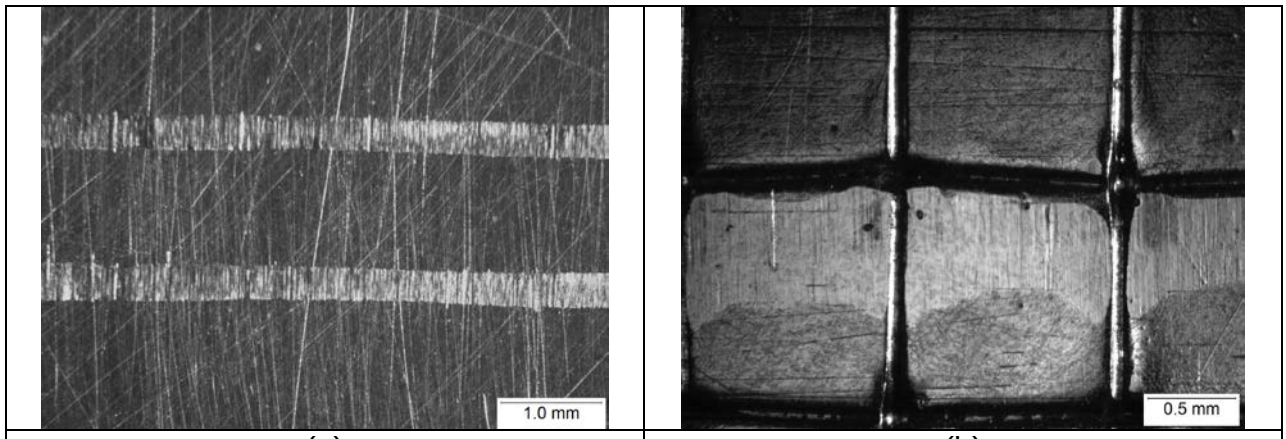

(a) (b)

Figure 4. Wear scars for two tests on a flat polished specimen (a) and a wear scar across the grid marks on a CTx specimen (b). Light scuffing can be seen in (b), but the wear seems more abrasive in nature on the tracks seen in image (a). Note that the magnification in image (b) is approximately twice that for (a).

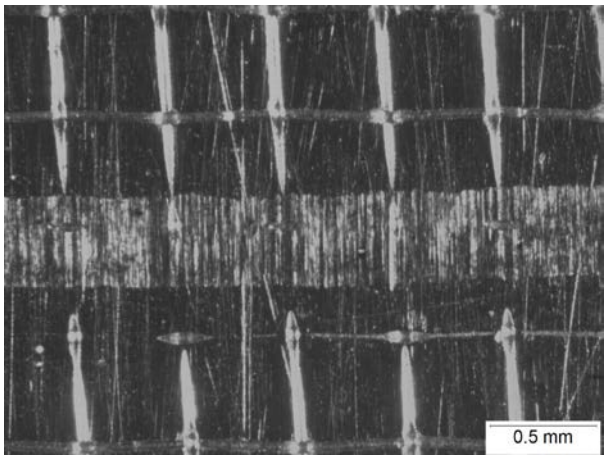

Figure 5. Wear scar for a VLBT test on a fine-textured surface showing light abrasion of the central features. Careful examination reveals tiny elliptical pockets that run alternatively vertically and horizontally within the worn area. These divots due to mesh cross-overs may have contributed to the friction reduction shown in Fig. 3.

Progress at George Washington University (subcontract). GWU has produced and sent four differently-textured piston ring segments to ORNL for frictional evaluation using ASTM Standard test method G181: "Standard Test Method for Conducting Friction Tests of Piston Ring and Cylinder Liner Materials Under Lubricated Conditions." Recognizing that piston ring sliding contacts operate over a range of speeds, loads, and temperatures during a single stroke, the test specimens, which contain arrangements of more than one type of geometric feature, are intended to optimize the beneficial effects of texturing over as wide a range of lubrication regimes as possible. They were delivered at the end of June, along with containers of mineral oil, tricresyl phosphate, and a commercial anti-oxidant. The latter additives are intended to provide stability to the mineral oil, but do not contain a full additive package, as would commercial fully-formulated lubricating oil. This mineral oil based fluid is the same formulation used by GWU in prior work on this project. Standardized friction tests of the four GWU-textured ring patterns against cast iron specimens that simulate honed cast iron cylinder liners will begin at ORNL during the next quarter.

Status of FY 2012 Milestones

1) (GWU subcontract) Submit report on the Cameron-Plint test procedure and the associated data for friction reduction under various conditions (12/31/2011). *Status: completed on schedule*.
2) (GWU subcontract) Develop a test procedure using an Atomic Force Microscope to measure the influence of nanoclay particles on the global mechanical properties of the clay infiltrated nanocomposites. Submit report containing an AFM test procedure in an ASTM standard format (1/31/ 2012). *Status: completed on schedule*.
3) (ORNL) Conduct lubricated friction tests using ASTM G181, and curved specimens with patterns found to offer the most promise for friction reduction and present a report on the results (6/30/12). *Status: textured piston ring specimens were received in June 2012 and testing will begin at ORNL during the coming quarter. The revised completion date for this task is projected to be 9/30/12.*
4) (ORNL) Working with a U.S. diesel engine manufacturer and George Washington University, develop a guideline report for applying textured surfaces to pistons and other promising components to affect fuel savings (9/30/12). *Status: this milestone is postponed until March 2013 due to a modification of the GWU subcontract for budget reasons*.

Communications/Visits/Travel

None

Problems Encountered

Initial plans included the provision of test specimens of textured surfaces to ORNL for testing in the spring of 2012; however, the GWU subcontract was only awarded in mid-FY 2011 and the production of test specimens was delayed. This was compounded by a reduction in funding and extension of the period of performance of the subcontract until March of 2013. This had the effect of postponing the completion of ORNL Milestone 3 for one quarter.

Publications/Presentations/Awards

None this quarter

References

1. P. J. Blau (2012) *Use of Textured Surfaces to Mitigate Sliding Friction and Wear of Lubricated and Non-Lubricated Contacts*, ORNL Tech Report ORNL/TM-2012/20, 19 pp.

Agreement 11752: Materials for High Efficiency Engines

Govindarajan Muralidharan and Bruce G. Bunting
Oak Ridge National Laboratory

Objective/Scope

To identify and catalog the materials operating conditions in the HCCI engines and utilize computational design concepts to develop advanced materials for such applications.

Technical Highlights

In this quarter, work was continued on Ni-based alloys for valve applications. As reported earlier, using thermodynamic modeling, microstructure evaluation, and mechanical property evaluation, high temperature fatigue was identified as a property of critical interest in Ni-based alloy valve materials for the next generation automotive engines. In order to develop relationships between the microstructures of the alloys and their mechanical properties, high-temperature fatigue property data were obtained on all down-selected alloys as a part of the project. Using the approximate correlation between the fatigue lives obtained using the rotating beam and fully reversed fatigue testing techniques several alloys with required microstructures have been identified as candidates for high temperature valve applications.

Using the microstructures of these alloys as a guide, computational thermodynamics was used to identify additional alloys with microstructure similar to the commercial alloys with desirable properties. In contrast to the commercially available alloys with high Nickel contents (> 75%), the Ni-content in these alloys ranges from about 30 wt % to 45 wt % with the potential to achieve comparable properties. This implies that the alloys will be of lower cost but comparable mechanical properties.

Results from the fatigue tests on newly developed alloys HCCI-9 and HCCI-16 showed that new alloys with greater strength levels were required to perform at 870°C and stress levels of 35 Ksi. Work continued in designing and fabricating new alloys aimed at increasing the strength levels. These alloys were vacuum arc cast into billets of size 1 in. x 1 in. x 3 in, rolled, heat-treated; Table 1 shows the newly developed alloys and their measured yield strengths at 870°C in the aged condition. It was concluded that further effort was required to achieve yield strengths of >75 Ksi.

This quarter further new alloys were designed with HCCI-16 as the basis. These alloys are modified versions of HCCI-16 reported in earlier reports in this project. Table 1 shows a significant improvement has been achieved in the yield strength of the alloys developed using the new design strategy. Note that an improvement of over 30%-40% has been achieved over the properties of the alloys designed in quarter 1, 2012. **The alloys designed in quarters 2 and 3 in 2012 have some of the highest strength levels achieved in this project**. It should be noted that the target of >75 Ksi yield strength has been achieved.

Alloy Designation	**Yield Strength at 870°C (Ksi)**
Quarter 1, 2012	
HCCI-490-1	65.4
HCCI-490-2	68.8
HCCI-490-3	66.7
HCCI-490-4	66.6
HCCI-490-5	63.5
HCCI-490-6	62.0
Quarter 2, 2012	
HCCI-41M3	78.5
HCCI-41M4	70.4
Quarter 3, 2012	
HCCI-161	**87.7**
HCCI-162	**82.3**
HCCI-164	**80.6**
Previous Results	
HCCI-41M	56.3

In addition, a large air melt of HCCI 41M3 and HCCI-200 was prepared for fatigue testing. Figure 1 shows a picture of the cast ingots.

Figure 1. Air cast 41M3 and HCCI-200.

Ingots will be rolled and fatigue testing will be initiated this quarter.

Status of FY 2012 Milestones:

(1) Complete rotating beam fatigue tests on at least two new alloys at 870°C, and stress greater than 25 Ksi. **(9/2012)** On Track

(2) Demonstrate a lifetime of >100 million cycles to failure at a stress level greater than 25 Ksi. **(9/2012)** On Track

Communications/Visits/Travel

Problems Encountered

The facility for casting large heats was inoperable and resulted in the delay of casting larger heats for fatigue testing

Publications/Presentations/Awards:

References

Agreement 13329: Design Optimization of Piezoceramic Multilayer Actuators for Heavy Duty Diesel Engine Fuel Injectors

H.-T. Lin, H. Wang, F.W. Zeng, A. A. Wereszczak,
Oak Ridge National Laboratory
and
R. Stafford and D. Memering
Cummins Inc.

Objective/Scope

Enable confident utilization of piezo stack actuator in fuel injectors for heavy vehicle diesel engines. The use of such actuators in diesel fuel injectors has the potential to significantly reduce injector response time, provide greater precision and control of the fuel injection event, and lessen energy consumption. Though piezoelectric function is the obvious primary function of lead zirconate titanate (PZT) ceramic stacks for fuel injectors, their mechanical reliability can be a performance and life limiter because PZT is intrinsically brittle, lacks of high strength, and is susceptible to fatigue-induced degradation and failure. However, that brittleness, relatively low strength, and fatigue susceptibility can be overcome with the use of appropriate probabilistic ceramic design methods.

Technical Highlights

1. Testing and Characterization of PZT Ceramics

1.2 Effect of humidity on flexural strength of PZT

PSI (Piezo Systems, Inc.) PZT was studied during this reporting period with an emphasis on the effect of humidity. Particularly, PSI 5A4E was used because this material had the piezoelectric properties equivalent to those of EPCOS PZT stacks currently down-selected for consideration for the fuel injectors in heavy duty diesel engine. Preparation of PZT specimens, specimen dimensions, and ball-on-ring (BoR) test conditions, including electric mechanical and electric loading, were all the same as those reported previously.[1,2] The study on the humidity effect was accomplished through pre-treating the PZT specimen in a chamber in a specified period of time. The chamber environment was controlled using potassium bromide solution at 81% R.H. (relative humidity), 22°C. Specimens with no treatment, treatments for 10 day, and one month were tested previously, and results were reported in previous quarterly report. Specimens with additional treatment period for up to five months were tested in this period. The weight gains of each group consisting of about 12 specimens after five months were about 1 mg. The data sets obtained for three electric conditions showed insignificant difference between the data sets of no humidity exposure and those of treated five months. The results are summarized in Fig. 1. The insensitivity of mechanical response to humidity up to 5 months indicates the excellent stability of the PZT materials in moisture environment at RT. However, further study on the

humidity aging effect at application temperature (~200°C) would be needed in order to confirm the long-term material stability under the application environment.

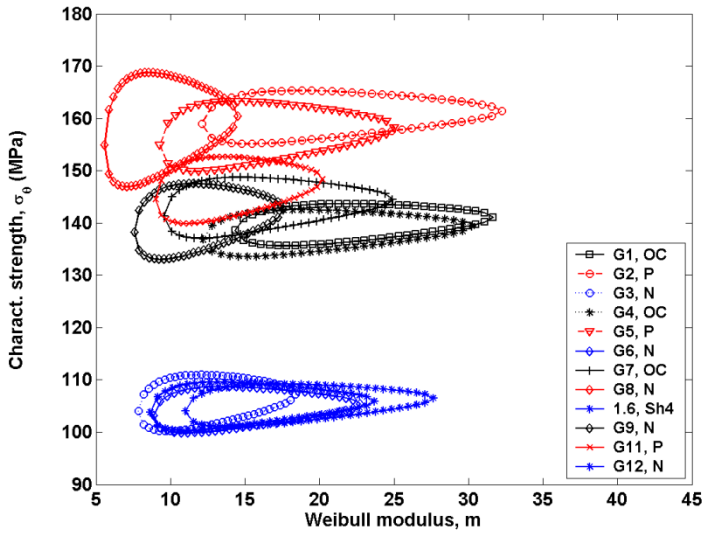

Fig. 1 Confidence ratio rings of mechanical strength of PSI 5A4E specimens in 95% confidence level. The results were obtained using BoR test. Data set G1-3: no humidity exposure (baseline data); G4-6: 10 days under 85% R.H.; G7-9: 1 month under 85% R.H.; G10-12: 5 months under 85% R.H. Each data set consisted of about 12 tests. OC: open circuit; P: electric field is along poling, 1.2 kV/mm; N: electric field is against poling, -1.2 kV/mm.

2. Testing and Characterization of PZT Stacks

2.1 EPCOS stacks

Testing on EPCOS PZT ceramics resorted to different configuration because the stand-alone single-layer PZT was not available; particularly, 10-layer plate specimens were used: 12 mm × 12 mm × 0.74 mm. The specimens were extracted from commercial EPCOS PZT stacks and supplied by Cummins Inc. Tests were conducted on BoR setup. However, the purpose of this study is to investigate the effect of temperature on the BoR flexural strength of 10-layer short stack. A self-aligning device that consisted of three-concentric alumina tubes was used for the mechanical testing. The inner tube was equipped with a protruded edge offering a supporting ring of ϕ9.5mm and outside tube was designed to host the plate specimen and an alumina ball of ϕ19.05mm. The latter served as a loading ball. Tests under high temperatures were carried out using the INSTRON bench top mechanical testing machine. A 20-minute soak-time was generally provided before the mechanical loading. Pre-load was controlled to be within 5 N. Loading Rate was maintained at 0.001 mm/s. The data set generated by the self-aligning BoR setup showed a characteristic flexural strength of 113.58 MPa. That is actuarially a little higher than one (104.65 MPa) obtained using the BoR setup with ϕ6.35 mm

steel ball and ϕ9.95 mm steel ring as reported before. It is not clear if it was due to the specimen preparation or test setup itself. However, the effect of temperature was apparently significant based on self-aligning BoR test, and that corresponded to 13 to 26 MPa decreases in flexural strength when the temperature was raised from room temperature to 100 and to 200°C as shown in Fig. 2. The fracture surfaces of 10-layer plates obtained in two temperatures are given in Fig. 3. The strength limiting flaws observed are typically surface pore or agglomerate.

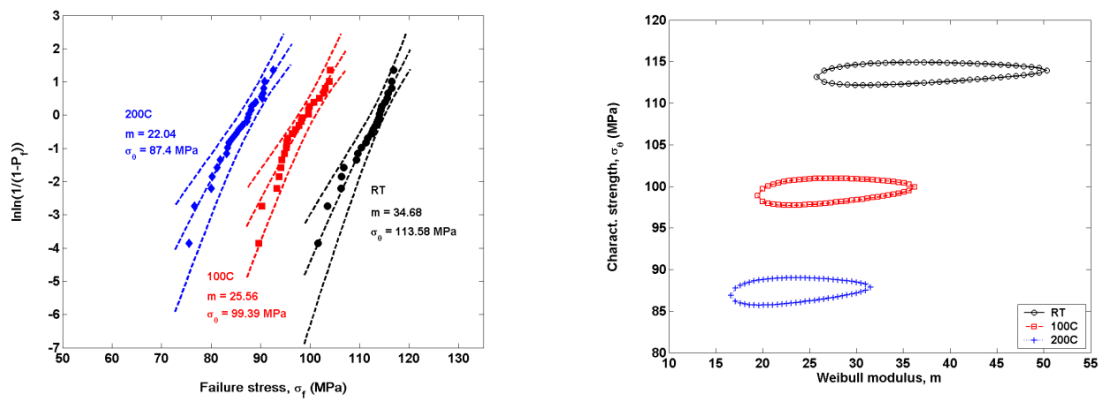

(a) (b)

Fig. 2 (a) Weibull plot of fracture stress based on BoR test of 10-layer plate specimens. (b) Confidence ratio rings of mechanical strength of 10-layer specimens in 95% confidence level.

In another series of tests, 16 bar specimens used for four-point bending were prepared from EPCOS stacks with the longitudinal axis along that of the stacks. (See Fig. 4) The specimens had a nominal size of 2.5 mm x 3.5 mm x 30 mm and bending tests were conducted with loading span of 6.35 mm and supporting span of 19.05 mm. The crosshead speed remained at a rate of 0.001 mm/s for all of the tests. The characteristic strength obtained of bar specimens was 26.88 MPa, which was ~ 23% lower than that (35 MPa) obtained for the similar bar specimens prepared out of EPCOS stacks in FY 2010. The fabrication and compositions of multilayer actuators might be responsible for the difference because these specimens were prepared actually from different configuration and/or size of EPCOS stacks. The failure usually took place on plate-to-bonding layer interface. Fracture was also observed crossing the PZT layers as shown in Fig. 5. However, it is hard to identify the location of failure origin associated with the fracture.

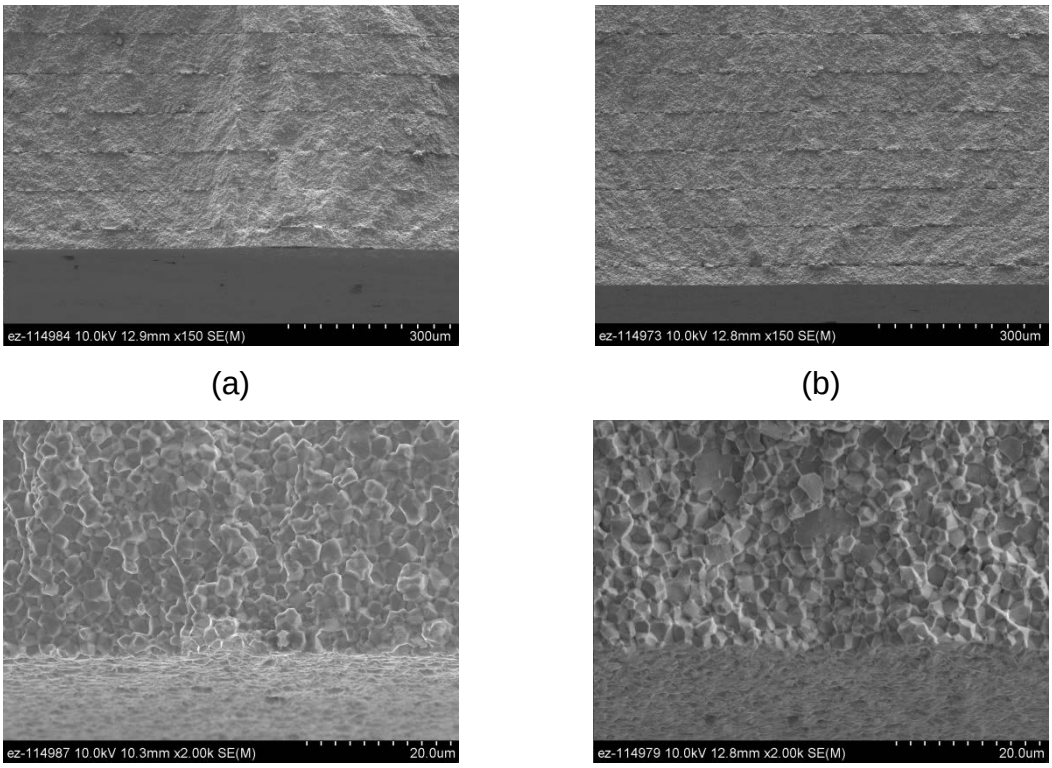

(a) (b)

(c) (d)

Fig. 3 Fracture surfaces of 10-layer stack showing aggregates in PZT layers as failure origin in 20°C (a) and (c) and 200°C (b) and (d).

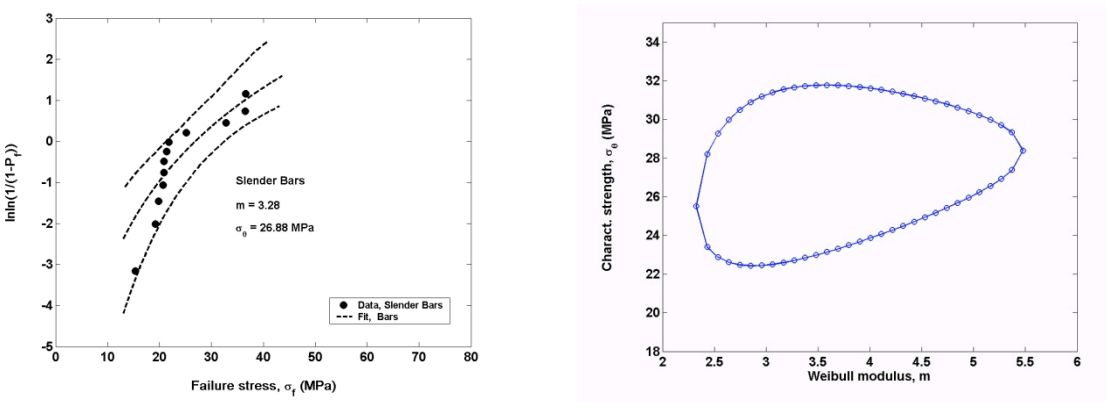

(a) (b)

Fig. 4 (a) Weibull plot of fracture stress based on four-point bending test of bar specimens. (b) Confidence ratio rings of mechanical strength of bar specimens in 95% confidence level.

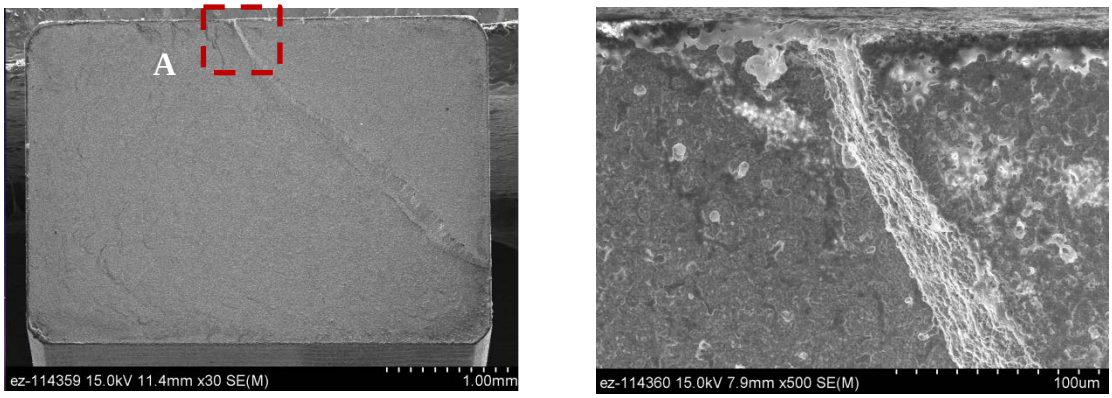

(a) (b)

Fig. 5 (a) Fracture surface of a bar specimen from four-point bending, and (b) enlarged and re-orientated local area A in (a). The specimen was prepared from an EPCOS stack.

2.2 Low-profile NOLIAC stacks using piezodilatometer

NOLIAC CMA09 stacks (10 mm × 10 mm × 2 mm, 440 nF, rated voltage 200 V) are currently being tested. Driving such size of stacks was enabled in the high electric field for the designed accelerating fatigue test because the current piezodilatometer was equipped with a Trek PZD 2000A that has a current capacity of ± 400 mA.

Measurements and cycling procedures mostly followed those established for single layer PZT, [3] but with some modifications with respect to the requirements testing of large size stacks.[4,5] Five electric cycle tests using 6 kV/mm at 100 Hz were completed. One of the stacks passed 10^6 cycles, whilst the rest stopped near 2.8×10^5 to 3.9×10^5 cycles. All of the stacks were found to be entirely breakdown and completely lost functionality. Additional electric cycle tests were performed including three under 3 kV/mm and one under 4.5 kV/mm. The fatigue and damaged actuators were also characterized using an impedance analyzer or small signal measurement. Fatigue data for NOLIAC stacks will be processed and prepared for the next quarterly report.

<u>Status of FY 2012 Milestones</u>

1. Complete study of the effect of humidity on the mechanical reliability of supplied down-selected and equivalent PZT ceramics. May 2012. ***Completed.***

2. Measure and compare reliability of competing commercially available piezoactuators under consideration for use in diesel fuel injectors. September 2012. ***On schedule*.**

<u>Communications/Visits/Travel</u>

Communications via e-mail and conference calls with Dr. R. Stafford Cummins, Inc. were maintained on CRADA updates.

Publications/Presentations/Awards

1. Zhang, K., Zeng, F.-W., Wang, H., and Lin, H.-T., Strength properties of aged poled lead zirconate titanate subjected to electromechanical loadings, submitted to *Smart Materials and Structures*, 2012.
2. Zhang, K., Zeng, F.-W., Wang, H., and Lin, H.-T., Biaxial flexural strength of poled lead zirconate titanate in high electric field with extended field range, submitted to *Ceramics International*, 2012.

References

1. Wang, H., Lin, H.-T., and Wereszczak, A. A., “Strength properties of poled lead zirconate titanate subjected to biaxial flexural loading in high electric field,” J. Am. Ceram. Soc., 93 (9), 2010, 2843-2849.
2. Wang, H. and Wereszczak, A. A., “Effects of electric field and biaxial flexure on the failure of poled lead zirconate titanate,” IEEE Trans. Ultras. Ferroelec. Freq. Contr., 55 (12), 2008, 2559-2570.
3. Wang, H., Matsunaga, T., Lin, H.-T., and Mottern, A. M., “Piezoelectric and dielectric performance of poled lead zirconate titanate in electric cyclic fatigue,” Start Materials and Structures, 21 (2), 2012, 025009.
4. Wang, H., Cooper, T. A., Lin, H.-T., and Wereszczak, A. A., “Fatigue responses of lead zirconate titanate stacks under semi-bipolar electric cycling with mechanical preload,” J. Appl. Phys., 108 (8), 2010, 084107.
5. Wang, H., Wereszczak, A. A., and Lin, H.-T., “Fatigue response of a PZT multilayer actuator under high-field electric cycling with mechanical preload,” J. Appl. Phys., 105 (1), 2009, 014112.

Agreement 17257: Materials for Advanced Turbocharger Designs

P.J. Maziasz and A. Shyam
Oak Ridge National Laboratory
and
K. Pattabiraman
Honeywell Turbo Technologies

Objective/Scope

This ORNL CRADA project with Honeywell, NFE-08-01671 (DOE/EERE/OVT Agreement 17257) began two years ago, and is scheduled to last for about 3 years. This CRADA project addresses the limitations of lifetime or use-temperature for the various components (casing, wheel, shaft, bearings) of both the turbine and compressor parts of the turbocharger system. As exhaust temperatures increase, to provide higher engine efficiency and lower emissions, turbocharger component temperatures also increase, so the need for more heat-resistant materials must be addressed. Requests for more detailed information on this CRADA project should be directed to Honeywell, Inc.

Highlights

Neutron-scattering experiments at ORNL to measure residual-stresses in critical locations of wheel/shaft assemblies and turbine housings are complete. Long-term creep-testing of cast CF8C-Plus austenitic stainless steel at 600°C continued this quarter, and aged specimens were tested this quarter. Assessments of the oxidation-resistance of CF8C-Plus steel relative to other exhaust component cast-irons and steels continued this quarter.

Technical Progress, 3rd Quarter, FY2012

Background

This CRADA project began two years ago, and will extend for 3 years, and covers several different tasks. The first task was to assess and prioritize the various components that need or would most benefit from materials upgrades to increase temperature capability and performance, as well as durability and reliability. The next tasks examine current performance and degradation modes of wheel/shaft assemblies for turbines and compressors, housings for turbines and compressors. These tasks may then obtain and test new materials with upgraded performance, and provide the results to Honeywell for designing advanced turbocharger systems, or for manufacturing of new prototype components for testing and evaluation.

Approach

This CRADA project began two years ago. This project is comprised of six tasks, which will span the next 36 month period. Activity began with ORNL and Honeywell discussing the priority of the various turbocharger components for materials upgrades. A turbocharger system includes the hot (turbine) end, driven by exhaust gas from the engine, a cold (compressor) end to increase air pressure into the combustion changer, and a transition region that connects these two ends. The turbine and compressor wheels are connected to a common shaft, supported by bearings. For the first task, the turbine wheel-shaft assembly was chosen as the first component for consideration, with analysis focused on residual stresses near the weld-joint of the Ni-based superalloy wheel to the steel shaft, which can upset rotational balance during service. Another task of this new CRADA project continues previous work between ORNL and Honeywell on testing of the new CF8C-Plus cast stainless steel as a significant performance upgrade for the turbine housings relative to standard SiMo or Ni-resist cast irons. This CRADA project for turbine housings covers a broad range of other high temperature properties, including creep and fatigue strength, and includes turbine housing applications for passenger vehicle gasoline engines.

Technical Progress

For Task 1, Honeywell identified neutron-scattering experiments to measure residual stresses in welded wheel/shaft assemblies as one of their highest priority items. For Task 2, these experiments were defined, and neutron scattering experiments at the HFIR Residual Stress User- Facility began previously. Preliminary neutron-scattering experiments for diffraction analysis of the steel shaft began previously, and additional experiments on wheel/shaft assemblies with variations in processing parameters continued and were completed last quarter. The results show asymmetric tensile hoop stresses in the as-welded condition.

For Task 3, ORNL continued long-term creep-rupture tests at 600°C of the cast CF8C-Plus stainless steel this quarter, with one test at 275 MPa rupturing after 7,300 h previously, and another test at 180 MPa continuing beyond about 17,860 h. ORNL completed aging of as-cast CF8C-Plus tensile/creep specimens at 700 and 800°C to 2500 h previously, and creep testing of the aged specimens at 700 and 800°C produced very short rupture lives this quarter. ORNL also completed additional longer-term creep-rupture testing at 700-850°C that have been added to previous creep-rupture data on CF8C-Plus and HK30-Nb steels. Honeywell is addressing the next steps necessary to commercially produce some prototype turbocharger housing using CF8C-Plus steel for the Ford 3.5L V-6 Ecoboost engine used in light trucks. This is the next step required so that new housings can be evaluated and tested on engines.

Oxidation experiments to assess the oxidation-resistance of cast CF8C-Plus relative to several cast-irons used for conventional turbochargers and exhaust system components began previously, and continued this quarter.

Communications/Visits/Travel

Periodic conference calls are held between ORNL and Honeywell Turbo Technologies, and email communications help to coordinate the work.

Status of Milestones (ORNL for DOE)

The FY2012 milestone to complete creep testing of the aged CF8C-Plus (04/2012) is complete and the milestone to extend the CRADA (08/2012) is on-track.

Publications/Presentations/Awards

None

Agreement 18570: Engine Materials Compatibility with Alternate Fuels

S. J. Pawel
Oak Ridge National Laboratory

Objective/Scope

The purpose of this Cooperative Research and Development Agreement (CRADA) between Oak Ridge National Laboratory and USCAR is to systematically evaluate compatibility between engine materials and ethanol fuel blends over a range of temperatures consistent with engine operation. Four primary tasks are included in the overall program:

1) surface analysis of materials exposed in field and lab exposures
2) in-situ extraction of gas and/or fluid from the valve seat crevice
3) development of electrochemical testing protocols
4) laboratory corrosion exposures of coupon materials

Technical Highlights

In the 3rd quarter of FY2012 a series of experiments was conducted involving immersion of aluminum specimens in a synthetic fuel blend (reference fuel C) with increasing concentrations of ethanol. Results indicated that the corrosion of commercially pure wrought aluminum as well as each of several cast aluminum alloys was a strong function of ethanol concentration, with increasing ethanol leading to rapidly accelerating corrosion. Figure 1 is a representative result, which shows the extent of corrosion of commercially pure wrought aluminum in a series of dry (<200 ppm water) fuel blend exposures for 24 h at 120˚C. Figure 1 shows that aluminum was essentially immune to corrosion in E0 for the conditions of this test, but that addition of as little as 5% ethanol (E5) resulted in isolated/shallow indications of corrosion. Increasing ethanol content lead to initiation of corrosion on increasingly large fractions of the specimen surface until, for E20, the entire surface was aggressively attacked in 24 h. In addition to the results depicted here, examinations were also conducted in E50, E85 and E100 for these conditions, all of which resulted in dissolution of the metallic specimen before the completion of the test period. Reaction products were found to include hydrogen gas, an amorphous combination of aluminum oxide, aluminum hydroxide and aluminum oxy-hydroxide. For the cast alloys, the corrosion products also included residual second phase material that does not appear to dissolve as the reaction proceeds, but rather remains behind in the growing areas of corrosion.

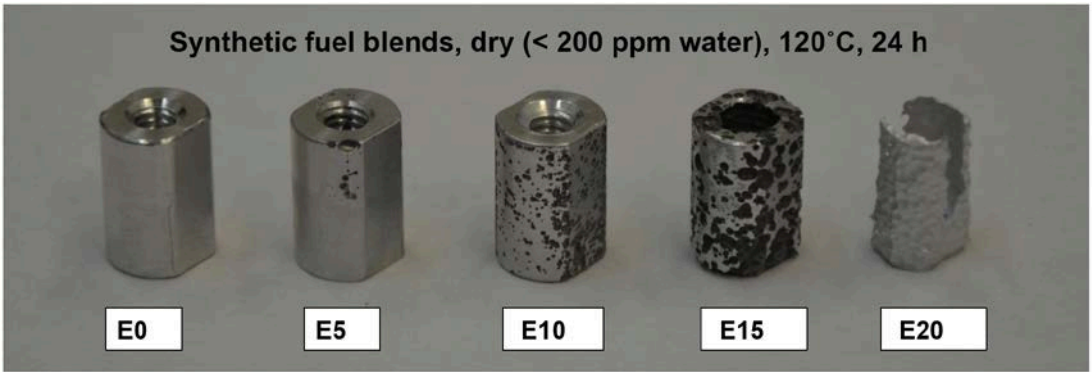

Figure 1. Corrosion of aluminum in increasing concentrations of dry ethanol synthetic fuel blend C at 120°C for a 24-hour time period.

Figure 2 is an example of corrosion progression as a function of time in dry ethanol conditions for an aluminum alloy at 78°C. This data indicates that the incubation time required for corrosion to begin was about 3 h for these conditions, but that once initiated, the corrosion reaction proceeded quite rapidly until most/all of the surface was actively corroding. Figure 3 shows high magnification SEM images of the reaction sequence for the specimens depicted in Figure 2. Small areas of active corrosion were observed to initiate and spread across the surface at a uniform rate (corrosion tends to grow radially from initiation points) until eventually, they overlapped as the entire surface activated. During this period, maximum weight loss rates were experienced by each specimen. However, at some point beyond 12 h exposure, the specimen started to regain mass as charcoal-black corrosion product, presumably aluminum ethylate, $Al(C_2H_5O)_3$, precipitated on the metal surface. The precipitation of corrosion products appears to slow the reaction rate considerably. This appears to be an effect of using a small volume of test fuel, which is rapidly saturated with dissolved species from the corrosion reaction. Under test conditions at higher temperatures or in larger volumes, this quenching effect has not been observed.

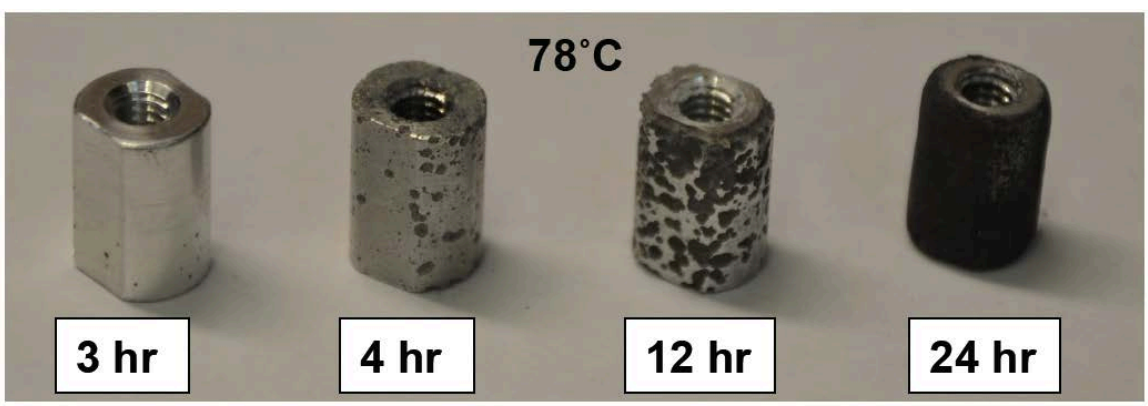

Figure 2. Aluminum alloy corrosion progression over a 24 hour time period. Specimens were exposed to anhydrous E100 at 78°C.

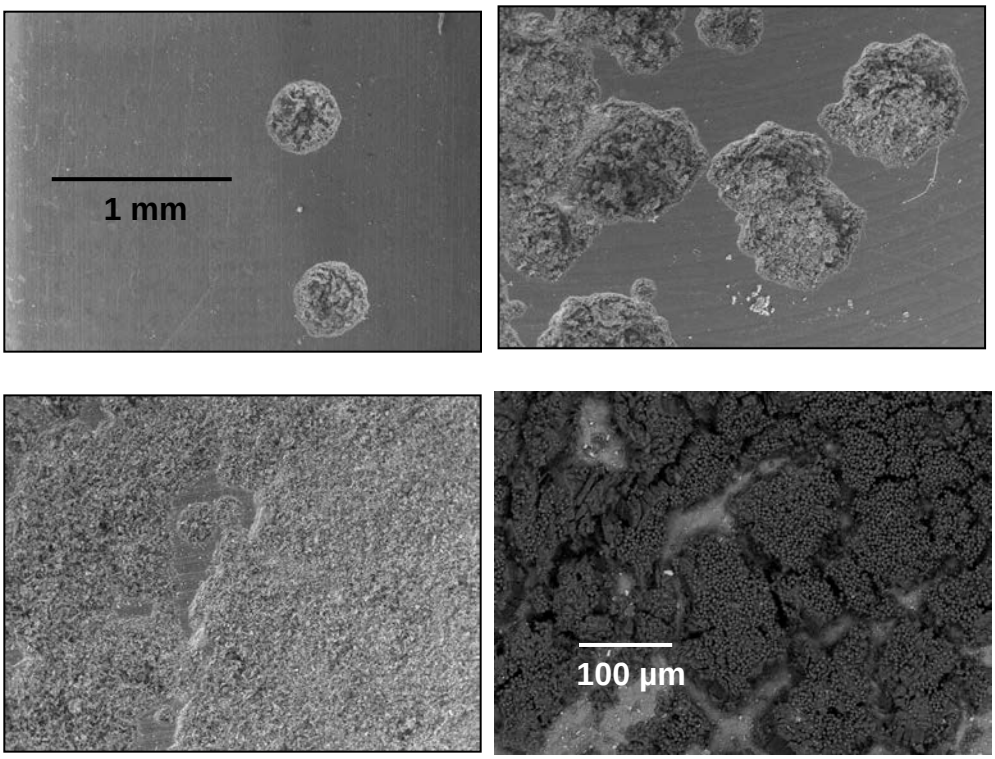

Figure 3. SEM images of aluminum alloy exposed to anhydrous E100 at 78°C for time periods corresponding to specimens in Figure 2.

Status of FY2012 Milestones
Ongoing

Communications/Visits/Travel
Routine electronic mail and regular telephone contact (bimonthly conference calls) is being maintained between the USCAR Partners and the ORNL team. A summary of recent results was presented at the DOE Annual Merit Review in Washington D.C. in May 2012.

Problems Encountered
None

Publications/Presentations/Awards
None to date. An open literature publication is in the final stages of preparation for submission to a Journal next Quarter.

References
None

Agreement 18571: Materials Issues Associated with Exhaust Gas Recirculation Systems

M. J. Lance, C. S. Sluder, M. K. Ferber and J. M. E. Storey
Oak Ridge National Laboratory

Objective/Scope

Provide information to industry specialists about fouling deposit properties so as to enable improved models and potential design improvements to reduce fouling and its impact on the performance of EGR (exhaust gas recirculation) coolers.

Technical Highlights

The temperature within the heat exchanger of our tube reactor was measured down the length in order to determine where the condensation of water would be likely to occur. Figure 1 shows the temperature measured from the outlet moving in to the tube for flow rates ranging from 5 to 20 SLPM. The temperature is lowest at the outlet where the gas has been cooled the most. The effect of the flow rate is shown in Figure 2. Two distinct regions are observed: at low flow rates the flow is laminar and so the temperature increases with flow rate due to the lower residence time of the gas. Above 10 SLPM, the flow is turbulent and the gas is more effectively cooled at higher flow rates. Experiments ongoing now will determine the location of water condensation using water sensitive strips.

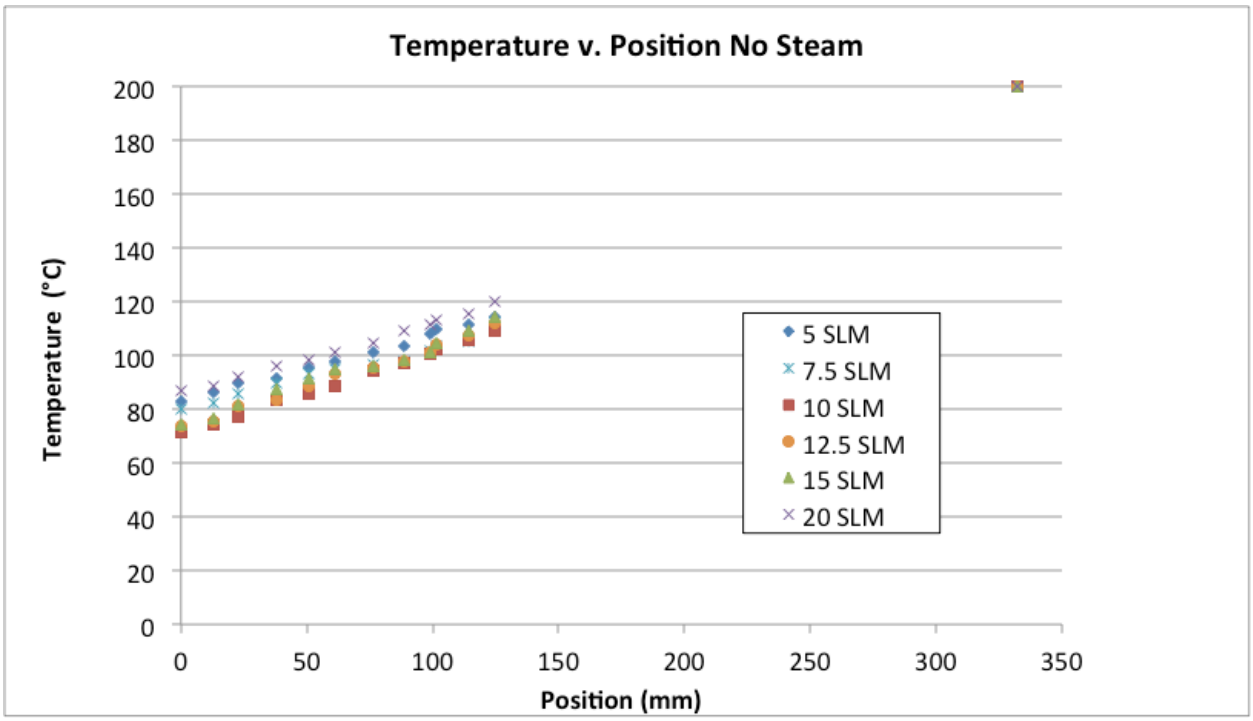

Figure 1. Temperature Profiles for 200°C Chamber Inlet, 22°C Coolant Temperature, and no Steam

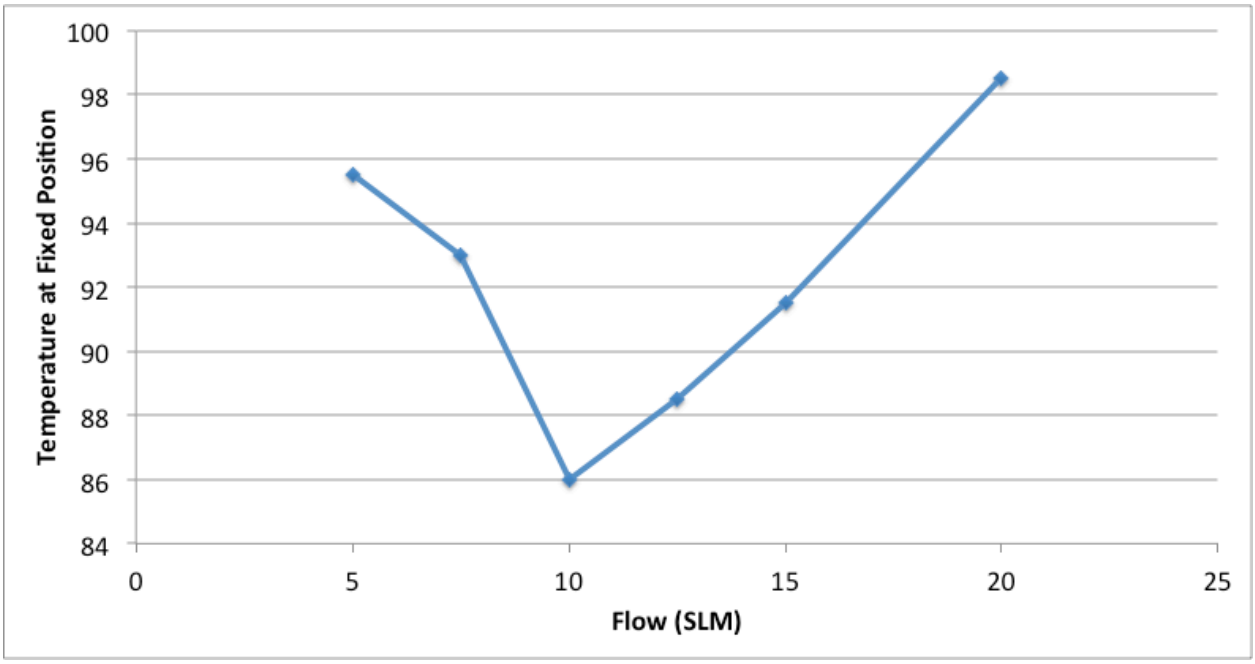

Figure 2. Transition in Heat Transfer Mechanism Observed as Flow Was Lowered

Parallel to the controlled laboratory aging of deposits, seven coolers have arrived for the second round of forensic deposit analysis from the industry consortium of EGR technicians. Deposits from plugged coolers had higher volatile fractions (up to 70%) compared to deposits from unplugged coolers suggesting a more important role for hydrocarbons and less importance of PM for EGR plugging. This is in contrast to the more commonly observed stabilized thermal-effectiveness loss of EGR coolers which contain deposits dominated by the string-of-pearls microstructure of PM. Moreover, at least two different types of EGR plugging deposits were observed (and have been reported by industry): lacquer-like and tar-like deposits.

Pyrolysis GC-MS revealed the composition of the lacquer-like deposits to be variants of 2, 3, and 4-ring polycyclic aromatic hydrocarbons (PAHs) and oxygenated PAHs with a narrow range of melting points and no fuel or paraffin peaks. These “proto-soot” compounds that have not lost all of the hydrogen necessary to become particulate carbon condense to form a brittle deposit at room temperature but will readily melt and coat the metal surface at temperatures expected within the EGR cooler during operation (see Figure 3). Conversely, tar-like deposits contained either or both oil and fuel components. Material and chemical deposit properties obtained from this study will enable improved understanding of EGR plugging in order to mitigate its effects on future engine platforms.

Figure 3. The image on the left is a lacquer-like deposit at 25°C. On the right, the same deposit at ~140°C after melting. Image width is 9 mm.

Status of FY2012 Milestones

1. Using facilities at the High Temperature Materials Laboratory, complete forensic analysis of industry-provided EGR cooler deposits in order to enable better understanding of fouling deposits properties for specific applications (i.e., an idling school bus) so as to meet Tier 4 emission standards of 0.40 g NO_x/kWh with no efficiency penalty. **(09/12)** *On Schedule*
2. Age laboratory-generated deposits (heavy-duty and light-duty) in controlled environments to investigate changes in deposit properties with the aim of increasing the baseline thermal conductivity of 0.04 W/mK to 0.2 W/mK by condensing water and/or HC on the deposit. **(09/12)** *On Schedule.*

Communications/Visits/Travel

None

Problems Encountered

None

Publications/Presentations/Awards

None

References

None

Agreement 10461: Durability of Diesel Engine Particulate Filters

Thomas R. Watkins, Amit Shyam, Hua-Tay Lin, Amit Pandey, Edgar Lara-Curzio
Oak Ridge National Laboratory
and
Randall J. Stafford
Cummins, Inc.

Objective

The objective of this effort is to identify and implement test techniques to characterize the physical and mechanical properties of ceramic diesel particulate filters (DPFs), to identify the mechanisms responsible for the degradation and failure of DPFs and to develop analysis tools for predicting their reliability and durability.

Goals, Barriers, Relevance & Integration

In the study area of OVT's Materials Technology subprogram, the Propulsion Materials Technology activity provides materials R&D expertise to enable advanced materials and supports the goals of several OVT subprograms.[1] Within the Advanced Combustion Engine subprogram-Combustion and Emission Control R&D activity, one *goal* is to: by 2015, develop materials, materials processing, and filter regeneration techniques that reduce the fuel economy penalty of particle filter regeneration by at least 25 percent relative to the 2008 baseline. This project addresses five *barriers* [1] related to the Emission Control: Lack of cost-effective emission control, improving durability and improving market perception. This project also addresses two *barriers* [1] related to the Propulsion Materials Technology activity itself: Changing internal combustion engine combustion regimes and reducing costly DPF failures. This project is *relevant* to the above goal as the understanding of the relationships of the material properties for the filter (and catalyst) substrates enables optimization of porosity, strength, elastic modulus, thermal conductivity, thermal expansion, etc. leading to improved materials processing and models and optimized regeneration strategies that improve fuel economy and increase DPF life. This project supports clean diesel, which increases acceptance by the public. Larger acceptance, in turn, results in larger percentages of conversion to diesel, with the resulting reduction in petroleum usage/dependency upon foreign oil. This project is *integrated* within Vehicle Technologies program as it utilizes characterization tools acquired and maintained by the High Temperature Materials Laboratory (HTML) Program.

Technical Highlights

The expected service lifetime of a typical DPF for on-road vehicles is >400 k miles, and the long-term durability of these devices hinges on their ability to withstand the stresses that are generated during operation, including transients such as filter regeneration. Regeneration refers to the process by which the accumulated particulate matter is removed from a filter. A typical regeneration approach involves heating the filter to combust the particulate matter trapped in the filter pores. Because the particulate matter combustion process is exothermic, a degree of control needs to be exercised during regeneration so that the stresses that result from thermal gradients do not lead to

mechanical failure of the filter. Increasingly stringent regulations for NOx, CO, and particulate matter emissions have prompted research activities to identify and develop materials capable of withstanding the conditions required to meet those regulations. These activities also include efforts to determine and understand the mechanical properties of these materials.[2]

In addition to the ~50% porosity in these materials, microcracking also plays an important role in their behavior. The unusual thermal expansion and high temperature elastic behavior of porous cordierite has been attributed to microcrack healing and re-initiation as a result of heating and cooling.[3] While this is an accepted mechanism, few researchers have provided evidence for crack healing at elevated temperatures in low thermal expansion ceramics. In the reporting period, the ORNL team continued characterizing the mechanical behavior of cordierite, aluminum titanate (AT)-based material and a β-eucryptite based material, investigating crack healing. This was accomplished by an iterative method, wherein, images of specific microstructural regions of a sample were recorded repeatedly after subsequent thermal treatments. After the initial SEM observation of a region, the specimen was heated at 5°C/min to 1100°C, held at this temperature for 24 h and subsequently cooled at 10°C/min to room temperature (see Figure 1). The sample was replaced in the SEM. The same areas were painstakingly relocated and imaged before and after the thermal cycle with the aid of fiducial features on the surface of the specimen. The observation of crack healing was performed, *ex-situ*. The changes in microcrack populations were recorded using backscattered SEM images in six regions of the specimen before and after heat treatment and again after a second identical thermal treatment.

Explicit evidence of change in crack population as a result of heating the DPF specimens to 1100°C is provided in Figures 2 - 4. The images on the left indicate the as-processed surface, and the corresponding image on the right is the same surface after the heat treatment. Images of the same area were taken after a second thermal cycle but are not shown. The grain-size range for the porous cordierite, AT-based and β-eucryptite based materials were measured to be 1.5-3, 5-10, and 1.5 - 7 µm by optical microscopy, respectively.

Figure 2 demonstrates that a microcrack in cordierite specimen present on the as-processed specimen surface has completely healed, and a new one has formed nearby with a small change in its orientation as a result of the thermal cycle. Similarly, Figure 3 shows a set of microcracks in the β-eucryptite based material where the larger cracks appear more open and the smaller cracks seem to close. In the center region of Figures 3A and B, an exhibition of crack healing and formation due to the thermal cycle is displayed. Likewise in Figure 4, a microcrack present in the as-processed aluminum titanate based material is completely healed in the upper left of the image. Taken together, the results in Figure 2- 4 provide compelling evidence of microcracks healing, evidence of change in microcrack population since new populations of microcracks have emerged as a result of elevated temperature exposure and subsequent cooling. Furthermore, it was observed that the second thermal cycle had a smaller effect on the microcrack distribution of cordierite materials as compared to the first cycle. These

results are in consistent with the Young's modulus dependence on thermal cycling where the largest decrease in Young's modulus is observed after the first thermal cycle.[3]

In summary, the role of microstructure is discussed with the thermal and elevated temperature mechanical properties of porous cordierite. Temperature cycling to 1000°C led to a net decrease in the Young's modulus although the decrease became smaller as a result of progressive cycling. The thermal expansion and Young's modulus of cordierite were strongly correlated in the temperature range examined due to the influence of microcracks in determining the value of both properties. Explicit evidence of microcrack healing and reopening was provided for the porous synthetic cordierite material.

Status of FY 2012 Milestones

In the reporting period, the ORNL team continued the determination of strength, fracture toughness, density/porosity/microstructure, and thermal expansion of coated DPFs as a function of time at elevated temperatures of 300, 500, 800 and 900°C for a second alternate substrate DPF material (SiC). Dynamic fatigue of samples tested at 0.000003 MPa/s will be conducted soon.

Travel and Presentations

ORNL and Cummins personnel traveled to Corning, NY to visit colleagues at Corning, Inc. on April 11-13, 2012 for technical discussions, presentations and tours of both the DPF research and manufacturing facilities there. ORNL personnel also traveled to Washington DC for the DOE 2011 Vehicle Technologies Annual Merit Review and Peer Evaluation Meeting on May 11, 2011 and made the following presentation:

T. R. Watkins, A. Shyam, H.T. Lin, E. Lara-Curzio, A. Pandey, R. Stafford, "Durability of Diesel Engine Particulate Filters," presented at the DOE 2012 Vehicle Technologies Annual Merit Review and Peer Evaluation Meeting, Washington, D.C., May 15, 2012.

References

1. Vehicle Technologies Program, Multi-Year Program Plan 2011-2015, Dec 2010, pp. 2.3-4, -5, -8; 2.5-7, -8, -9, -10.
2. A. Shyam, E. Lara-Curzio, T. R. Watkins and R. J. Parten, "Mechanical Characterization of Diesel Particulate Filter Substrates," *J. Am. Ceram. Soc.*, **91** [6] 1995–2001 (2008).
3. A. Shyam, E. Lara-Curzio, A. Pandey, T. R. Watkins, K. L. More, "The Thermal Expansion, Elastic and Fracture Properties of Porous Cordierite at Elevated Temperatures," *J. Am. Ceram. Soc.*, **95** [5] 1682–1691 (2012).

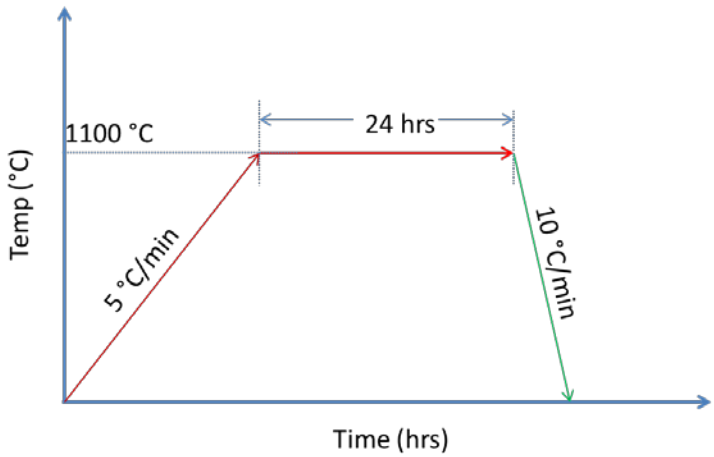

Figure 1 – Schematic of thermal cycling.

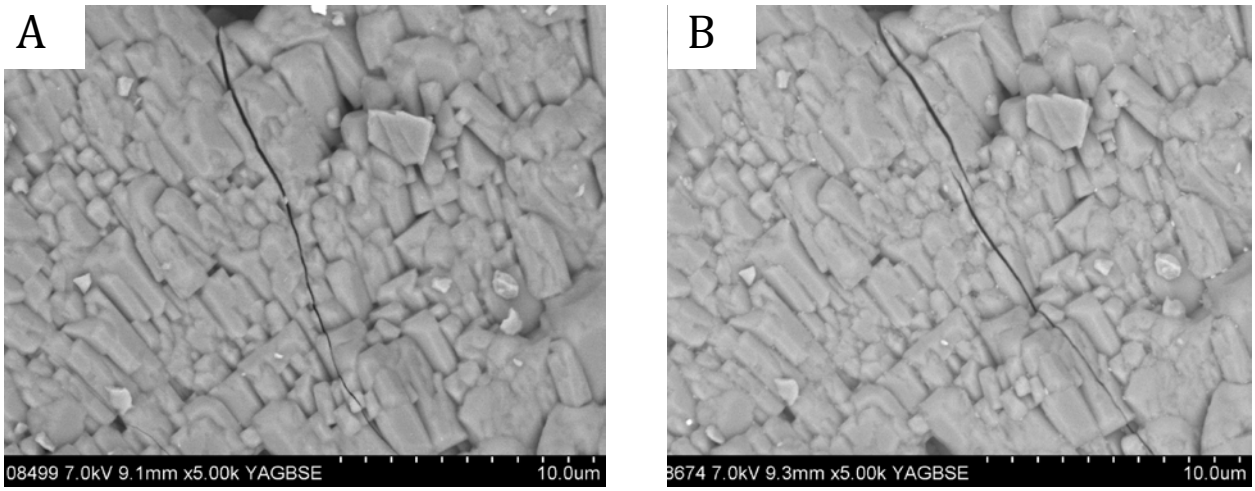

Figure 2 – SEM micrograph of Cordierite A) before and B) after thermal cycling.

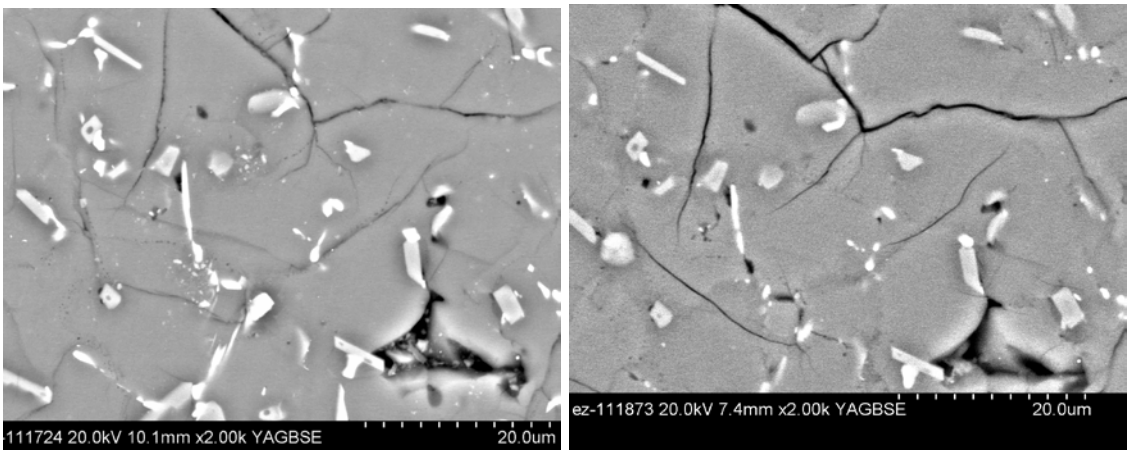

A.) B.)

Figure 3 – SEM micrograph of β-eucryptite A.) before and B.) after thermal cycling.

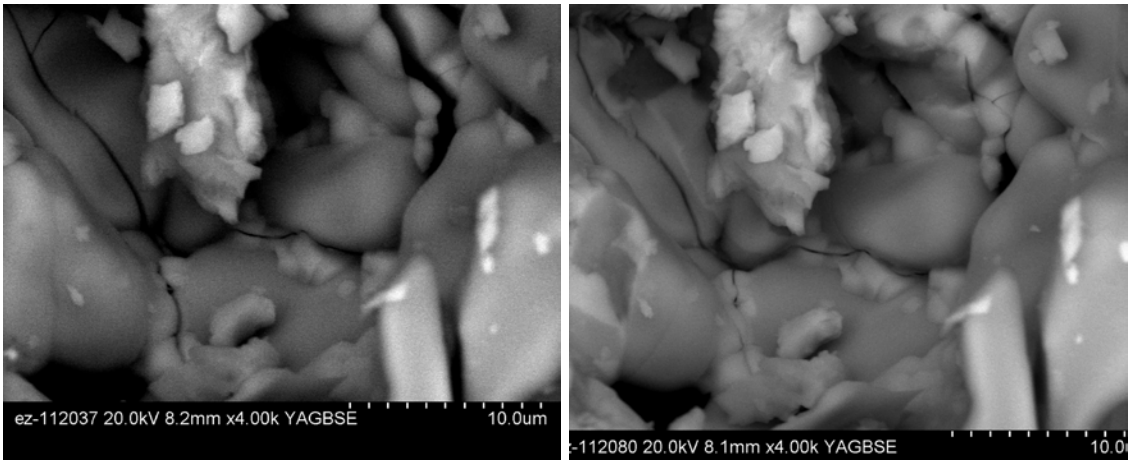

A.) B.)

Figure 4 – SEM micrograph of Aluminum titanate based DPF A) before and B) after thermal cycling.

Agreement 10635: Catalysis by First Principles

C. Narula, M. Moses DeBusk
Oak Ridge National Laboratory

Objective/Scope

This research focuses on an integrated approach between computational modeling and experimental development, design and testing of new catalyst materials, that we believe will rapidly identify the key physiochemical parameters necessary for improving the catalytic efficiency of these materials. The results will have direct impact on the optimal design, performance, and durability of supported catalysts employed in emission treatment; e.g., lean NO_x catalyst, three-way catalysts, oxidation catalysts, and lean NO_x traps etc.

The typical solid catalyst consists of nano-particles on porous supports. The development of new catalytic materials is still dominated by trial and error methods, even though the experimental and theoretical bases for their characterization have improved dramatically in recent years. Although it has been successful, the empirical development of catalytic materials is time consuming and expensive and brings no guarantees of success. Part of the difficulty is that most catalytic materials are highly non-uniform and complex, and most characterization methods provide only average structural data. Now, with improved capabilities for synthesis of nearly uniform catalysts, which offer the prospects of high selectivity as well as susceptibility to incisive characterization combined with state-of-the science characterization methods, including those that allow imaging of individual catalytic sites, we have compelling opportunity to markedly accelerate the advancement of the science and technology of catalysis.

Computational approaches, on the other hand, have been limited to examining processes and phenomena using models that had been much simplified in comparison to real materials. This limitation was mainly a consequence of limitations in computer hardware and in the development of sophisticated algorithms that are computationally efficient. In particular, experimental catalysis has not benefited from the recent advances in high performance computing that enables more realistic simulations (empirical and first-principles) of large ensemble atoms including the local environment of a catalyst site in heterogeneous catalysis. These types of simulations, when combined with incisive microscopic and spectroscopic characterization of catalysts, can lead to a much deeper understanding of the reaction chemistry that is difficult to decipher from experimental work alone.

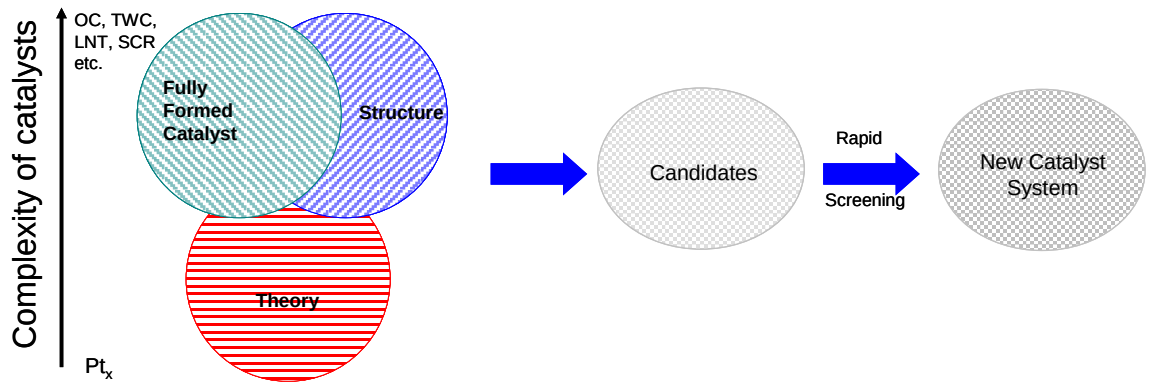

Thus, a protocol to systematically find the optimum catalyst can be developed that combines the power of theory and experiment for atomistic design of catalytically active sites and can translate the fundamental insights gained directly to a complete catalyst system that can be technically deployed.

Although it is beyond doubt computationally challenging, the study of surface, nanometer-sized, metal clusters may be accomplished by merging state-of-the-art, density-functional-based, electronic-structure techniques and molecular-dynamic techniques. These techniques provide accurate energetics, force, and electronic information. Theoretical work must be based on electronic-structure methods, as opposed to more empirical-based techniques, so as to provide realistic energetics and direct electronic information.

A computationally complex system, in principle, will be a model of a simple catalyst that can be synthesized and evaluated in the laboratory. It is important to point out that such a system for experimentalist will be an idealized simple model catalyst system that will probably model a “real-world” catalyst. Thus it is conceivable that “computationally complex but experimentally simple” systems can be examined by both theoretical models and experimental work to forecast improvements in catalyst systems.

We have focused on the oxidation catalyst and SCR catalyst to develop and demonstrate catalyst by design protocol as a prelude to developing catalyst by design protocols for complex emission treatment catalysts; e.g., TWCs, NO_x traps, and HC-SCR catalysts. Our goals are as follows:

- Our theoretical goal is to carry out the calculation and simulation of realistic supported Pt nanoparticle systems (i.e., those equivalent to experiment), in particular by addressing the issues of complex cluster geometries on local bonding effects that determine reactivity. As such, we expect in combination with experiment to identify relevant clusters, and to determine the electronic properties of these clusters. In addition, we plan to study zeolite structures with a view to develop an insight on the mechanistic aspects of catalytic process to enable us to develop better catalysts.
- Our experimental goal is to synthesize metal carbonyl clusters, decarbonylated metal clusters, sub-nanometer metal particles, and metallic particles (~5 nm) on

alumina (commercial high surface area, sol-gel processed, and mesoporous molecular sieve), characterize them employing modern techniques including Aberration Corrected Electron Microscope (ACEM), and evaluate their CO, NO_x, and HC oxidation activity. Furthermore, guided by theoretical studies we plant to synthesize new zeolites and characterize them.

- This approach will allow us to identify the catalyst sites that are responsible for CO, NO_x, and HC abatement. We will then address design of new durable catalysts systems that can withstand the prolonged operations.

Technical Highlights

In the previous quarterly report, we summarized our theoretical modeling and experimental results on CO oxidation on single Pt atoms supported on θ- and γ- Al_2O_3. This work is complete and answers the question whether single supported Pt atoms can catalyze reactions. Previous literature reports in single atom catalysis are limited to Pd/MgO and Pt/Fe_2O_3 systems. In both cases, the substrate participates in the reaction enabling classing Langmuir-Hinshelwood pathways to occur during catalyzed oxidation reactions. Unlike MgO and Fe_2O_3, alumina is inert and cannot participate in oxidation reaction. As such, we also propose s variation of Langmuir-Hinshelwood oxidation mechanism based on first principles theoretical models. The manuscript based on this work is nearing completion and will be submitted for publication in the next quarter.

Our initial experimental work on low-temperature NH3-SCR (supported by AMO) is being completed under this project since this project provided modeling support to the project. At present, the characterization of a new catalyst which exhibits unprecedented high NOx conversion at 150C and is hydrothermally stable is being completed in response to the reviewers' comments who have recommended the publication of the manuscript in J. Phys. Chem. C. The results are summarized in this report.

We also summarize advances made on Pt agglomeration dung this quarter as well as ongoing efforts to explain the role of Pd in reducing Pt-Pd agglomeration to extremely large particles during hydrothermal aging.

Structural Characterization of CuFe-SSZ-13

The samples of CuFe-SSZ-13, prepared by ion exchange with iron nitrate at 80C and subsequent thermal treatment, exhibit high NOx conversion activity as compared with Cu-SSZ-13. Here, Cu-SSZ-13 is a commercial urea-SCR catalyst. The performance of Cu-SSZ-13 and CuFe-SSZ-13 is identical in 200-650C range. After hydrothermal aging, CuFe-SSZ-13 retains it high NOx conversion activity at 150C.

The UV-Vis of Cu-SSZ-13 and CuFe-SSZ-13 is shown in Figure 1. The UV-Vis spectrum of (Figure 1) CuFe-SSZ-13 and Cu-SSZ-13 exhibit a very intense absorption from a d-d transitions at ~ 210 nm and a broad peak at ~ 830 nm from the charge transfer band related to O → Cu transition from lattice oxygen to isolated Cu^{2+} ions. In addition, CuFe-SSZ-13 has two absorptions that can be attributed to isolated tetrahedral and octahedral Fe^{3+}, at 210 and 270 nm, respectively, as seen in Fe-ZSM-5 type

structures. In general, absorptions of iron oxide clusters and iron oxide particles are believed to be above 400 nm and are not seen.

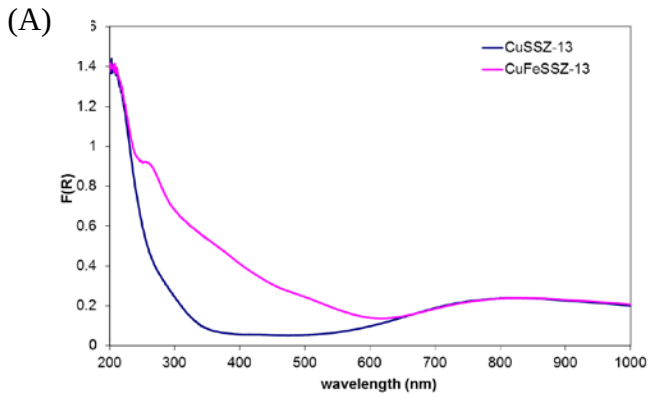

Figure 1. Diffuse reflectance UV-Vis of Cu-SSZ-13 and CuFe-SSZ-13

A new, intense absorption centered at ~ 350 nm (Figure 1A) is also present which could be assigned to octahedral Fe^{3+} in small oligomeric clusters and has previously been assigned to $[HO\text{-}Fe\text{-}O\text{-}Fe\text{-}OH]^{2+}$ cluster bound to the zeolite framework via iron oxygen bridges.

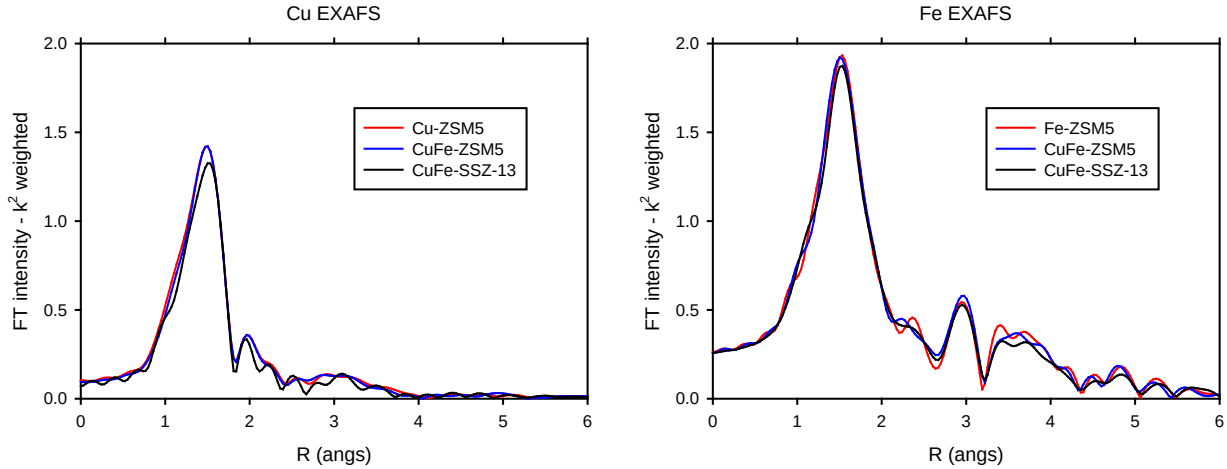

Figure 2: EXAFS of Cu-SSZ-13 and CuFe-SSZ-13

The Cu EXAFS and XANES of CuFe-SSZ-13 are identical to those of Cu-SSZ-13 and the data suggest Cu to be Cu(II) [Figure 2]. The Fe EXAFS and XANES of CuFe-SSZ-13 could not be compared to Fe-SSZ-13 but the data indicate a structure very similar to that of Fe-ZSM-5 and Cu-Fe-ZSM-5. These data point to a structure where

Cu is in ionic position in Cu-SSZ-13 whereas iron reside sin the pores of Cu-SSZ-13 as an oligomeric cluster.

Sintering of Pt atoms on Pt/θ-alumina (010) surface

The sintering of platinum particles has been extensively studies and some of the models developed for Pt particles also apply to Pt nanoparticles. Theoretical studies point to structures of various small clusters and show that oxidized Pt is more prone to sintering. However, the reasons for facile sintering of Pt particle are not well understood. It is in this context we started our work to understand the reason for sintering with the expectation that insights will help us design the catalyst materials that are less susceptible to sintering. We have completed the study of 2 and 3-atom systems. We find that there is no significant difference between binding energy of two atom clusters and two independent atoms. For three-atom clusters, the clusters are more energetically favored over three independent atoms. The results on 2-3 and three atom clusters were summarized in the last report. In this report, we describe our results in 4-atom systems.

Four Pt atom clusters: The total energy of 4 atoms absorbed on θ-alumina 110 surfaces is -3054.4954 eV. These four atoms are independent of each other and each of these atoms is located above aluminum and bonded to two oxygen atoms on the surface. All platinum atoms are d^{10} species (Figure 3).

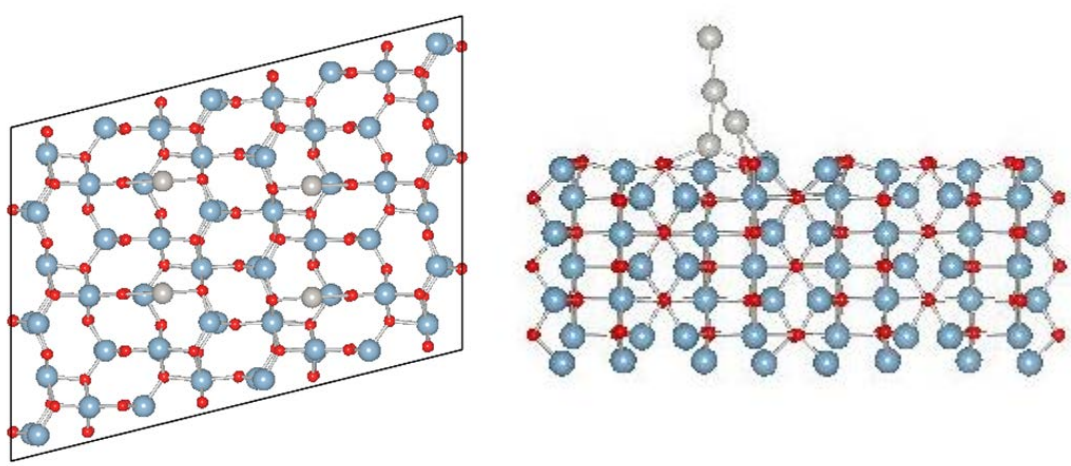

Figure 3: Four Pt atom and cluster supported on θ-alumina 110 surfaces

The four atom cluster, on the other hand is favored by 78.3 Kcal/mol over four atoms adsorbed on θ-alumina 110 surfaces. Its total energy is -3057.8930 eV and all Pt atoms are d^9.

These results confirm that increased stability of clusters over supported independent atoms provides the driving force for sintering. The detailed analysis of 2,3- and 4-atom clusters will be presented in the next report.

Pt-Pd/Alumina system:

We have previously shown that pre-formed Pt-Pd nanoclusters with Pt-Pd ratio of 3:1, 1:1, and 1:3 supported on γ-alumina are hydrothermally more stable than Pt/γ-alumina in 500-900C range and do not form extra-large clusters of 300-400 nm commonly observed upon hydrothermal aging of Pt/γ-alumina. In order to explain the phenomenon, we are carrying out first principles modeling of four atom cluster, Pt3Pd/γ-alumina, and the optimized structures are shown in Figure 4.

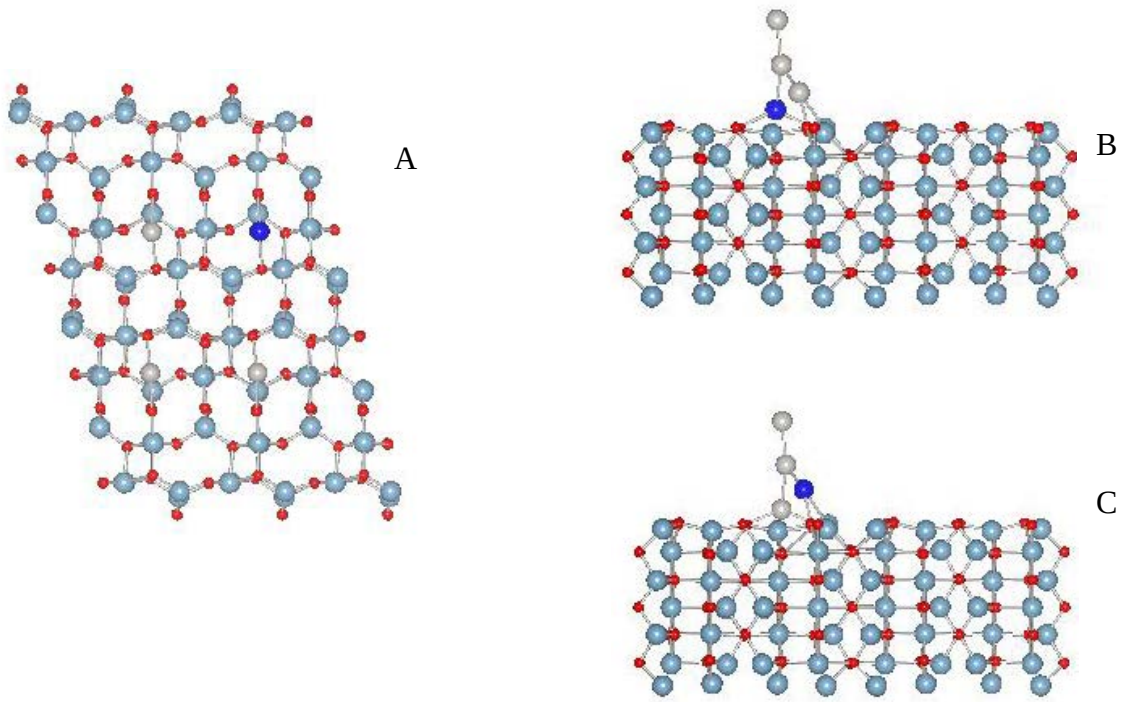

Figure 4: Pt3Pd cluster supported on θ-alumina 110 surfaces [Pd atom is dark blue and Pt atoms are gray]

The total energy of the system where three platinum and one palladium atoms are adsorbed on θ-alumina 110 surfaces is -3054.4628 eV (A) and all atoms are d10. In 4 -atom clusters where cluster bonding to θ-alumina 110 surfaces occurs via one platinum and one palladium, the energies are -3055.7018 eV (B) and -3055.2498 eV. The optimization of other two configurations of 4-atom cluster (Pd in the middle and Pd on surface) is still in progress and the results will show energetically favored location for Pd.

Status of FY2012 Milestones:

1. We will complete theoretical modeling of large supported Pt clusters by Sept 2012 resulting in a thorough understanding of subnanometer Pt and Pt clusters supported on alumina.

   We have completed modeling of 2-4 atom clusters and analysis is in progress.

2. This information will be used to initiate mechanistic studies of CO oxidation are nearing completions. The NO_x and HC oxidation on Pt/alumina and heterobimetallic zeolites will be initiated in the next quarter.

Communication/Visits/Travel

We have published a manuscript titled "Ab Initio Density Functional Calculations of Adsorption of Transition Metal Atoms on θ-Al_2O_3(010) Surface" Journal of Physical Chemistry, C. Another manuscript titled "Heterometal Incorporation of M-Exchanged Zeolties enables low temperature catalytic activity of NOx reduction" has been recommended for publication by reviewers. A third manuscript titled "CO Oxidation on Supported Single Pt Atom – Experimental and *Ab Initio* Density Functional Studies of CO interaction with Platinum Atom on θ-Al_2O_3(010) Surface" is being prepared for submission to J. Am. Chem. Soc.

Problems Encountered

None

Publications

1. X. Yang, Z. Wu, M.M. DeBusk, D.R. Mullins, S.M. Mahurin, R.A> Geiger, M. Kidder, C.K. Narula, Heterometal Incorporation of M-Exchanged Zeolties enables low temperature catalytic activity of NOx reduction, J. Phys. Chem. C (all reviewers recommend publication – manuscript is being revised in response to comments)
2. C.K. Narula, M.G. Stocks, "Ab Initio Density Functional Calculations of Adsorption of Transition Metal Atoms on θ-Al_2O_3(010) Surface" J. Phys. Chem,. C, 2012, 116, 5628.
3. C.K. Narula, "Catalyst by Design – Bridging the Gap between Theory and Experiments at Nanoscale Level" Encyclopedia of Nanoscience and Nanotechnology, Vol. II, Taylor & Francis, New York, 2008, pp 771-782 (invited).
4. C.K. Narula, L.F. Allard, D.A. Blom, M. Moses-DeBusk, "Bridging the Gap between Theory and Experiments – Nano-structural Changes in Supported Catalysts under Operating Conditions" SAE-2008-01-0416, SAE Int. J. Mater. Manu., 1(2008) 182-188.
5. C.K. Narula, L.F. Allard, D.A. Blom, M.J. Moses, W. Shelton, W. Schneider, Y. Xu, "Catalysis by Design - Theoretical and Experimental Studies of Model Catalysts", SAE-2007-01-1018 (invited).

6. C.K. Narula, M.J. Moses, L.F. Allard, “Analysis of Microstructural Changes in Lean NO_x Trap Material Isolates Parameters Responsible for Activity Deterioration” SAE 2006-01-3420.
7. Y. Xu, W.A. Shelton, and W.F. Schneider, “The thermodynamic equilibrium compositions, structures, and reaction energies of Pt*x*O*y* (*x* = 1-3) clusters predicted from first principles,” *Journal of Physical Chemistry B,* 110 (2006) 16591.
8. Y. Xu, W. A. Shelton, and W. F. Schneider, “Effect of particle size on the oxidizability of platinum clusters,” *Journal of Physical Chemistry A*, 110 (2006) 5839.
9. C.K. Narula, S. Daw, J. Hoard, T. Hammer, “Materials Issues Related to Catalysts for Treatment of Diesel Exhaust,” *Int. J. Amer. Ceram. Tech*., 2 (2005) 452 (invited).

Presentations (last 12 months)

1. Narula, C.K. Stocks, G.M., Density Functional Studies of Adsorption of Transition Metal Atoms on θ-Al_2O_3(010) Surface” American Chemical Society Meeting, Denver, CO, August 28, 2011.
2. Narula, C.K.; Stocks, M. G.; First-principles studies of the structure and bonding of metal atoms supported on θ-alumina, American Chemical Society Meeting, San Francisco, March 2010.
3. Narula, C.K.; Chen, X.; Stocks, G.M., DeBusk, M.M.; Allard, L.F.; “First-Principles and Experimental Studies of the Sub-Nanomenter Platinum Atoms Supported on θ-Alumina” 230th American Chemical Society Meeting, Boston, MA, August 22-26, 2010

References

1. Cheng, P.T.; Cook, C.D., Nyburg, S.C., Wan, K.; Can. J. Chem., 49 (1971) 3772.
2. Scholz, S.; Lerner, H.W.; Bolte, M. Acta Cryst E62 (2006) m312-m313. Gregg, M.R.; Powell, J.; Sawyer, J.F.; Acta. Crystal. C44 (1988) 43-46
3. Qiao, B; Wagn, A.; Yang, X.; Allard, L.F.; Jiang, Z.; Cui, Y.; Liu, J.; Li, J.; Zhang, T.; Nature Chem., 3 (2011) 634

Agreement 19214: Effects of Biodiesel Fuel on Diesel Particulate Filter Materials

M. J. Lance, B. J. Bunting, A. A. Wereszczak, M. K. Ferber, E. E. Fox, and T. J. Toops
Oak Ridge National Laboratory

Objective/Scope

To characterize changes in the microstructure and material properties of diesel particulate filters (DPFs) in exhaust gas produced by biodiesel blends.

Technical Highlights

To gain some perspective of what positional, coefficient of thermal expansion (CTE) differences could exist in the SiC DPF material, measurements were made with an available cordierite DPF. Effect of temperature cycling was also examined. The CTEs were all relatively low and increased similarly with an increase in temperature as shown in Fig. 1. However, the CTE for coupons harvested out of the longitudinal orientation showed ~~that~~ the CTE to be negative below approximately 200°C. Similar measurements are now underway in Q4 with a SiC DPF that was exposed to various combustion environments.

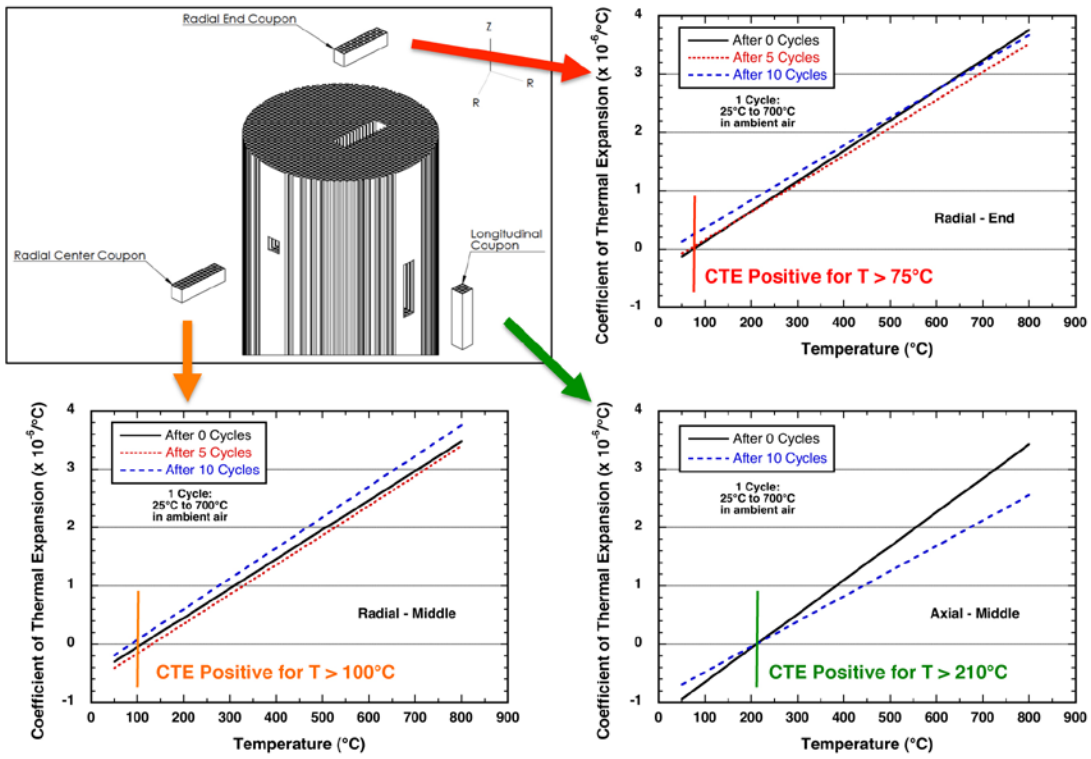

Figure 1. Coefficient of thermal expansion as a function of orientation, temperature, and cycling conditions.

The apparent thermal conductivity of a SiC DPF was measured in its axial direction using a hot-disk thermal constants analyzer. Numerous tests were run and the apparent thermal conductivity for all of them ranged between 2 to 4.5 W/mK.

Efforts are continuing to develop a tensile test method for DPFs as well as a suitable specimen geometry. Examples of considered tensile test coupons are shown in Fig. 2, and the mounting of a coupon in tensile grips are also shown. There are several advantages to tensile testing over other (bend or compression) test methods. Coupled with the measurement of tensile elongation, the sought-after tensile testing will enable the measurement of a continuous tensile stress - tensile strain curve. Such definitive data will allow for the interpretation of non-linear tensile response, and provide critical information on the (continuous or tangent) elastic modulus as a function of tensile strain. An example of a measured tensile response is shown in Fig. 3.

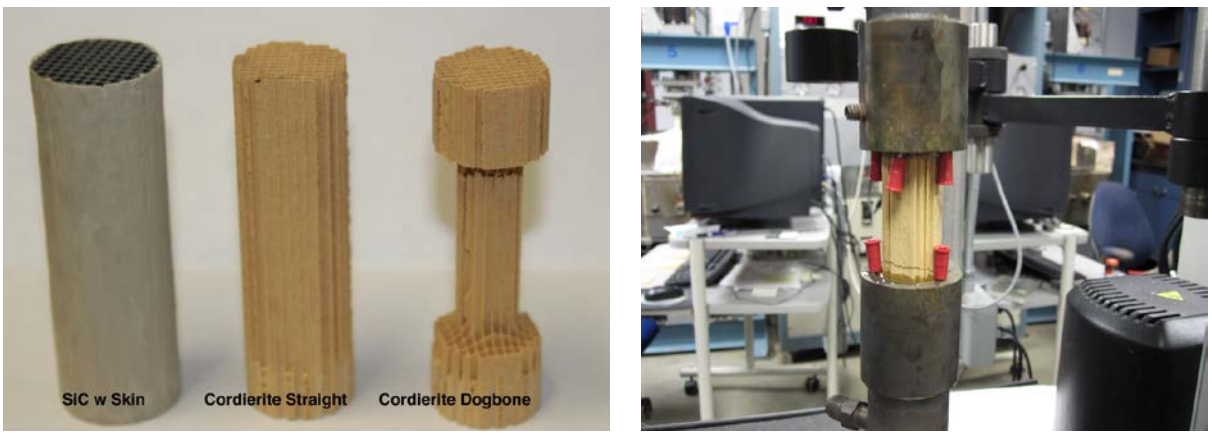

Figure 2. Examples of considered tensile test coupons (left) and their mounting in grips for tensile testing (right).

Biaxial flexure testing was started to examine if high temperature exposure to different fuel environments (having different alkali or alkaline earth additives) and resulting ash condensation will affect failure stress. An example of the test setup is shown in Fig. 4. The testing will be completed in early Q4, and their results will aid in the interpretation of how these different species affect SiC DPF mechanical response.

Lastly, in order to more efficiently conduct engine experiments with a variety of fuel blends, an auxiliary fueling system was designed. This external fuel system combines 4 separate tanks in a manifold arrangement. With a multiport selector valve, any one of 4 fuels may be chosen. Thought was taken to ensure streamlined fuel changeovers with low downtime and no fuel cross-contamination, by means of staged drain paths with easy access, remote fill neck assemblies, and a self-priming lift pump. The fuel setup is shown in Figure 5. Electrical static discharge within the multiple fuel streams was eliminated with helical wrapping of the fuel pipes with a copper conductor, and tailoring the fluid flow velocities in the supply and return streams.

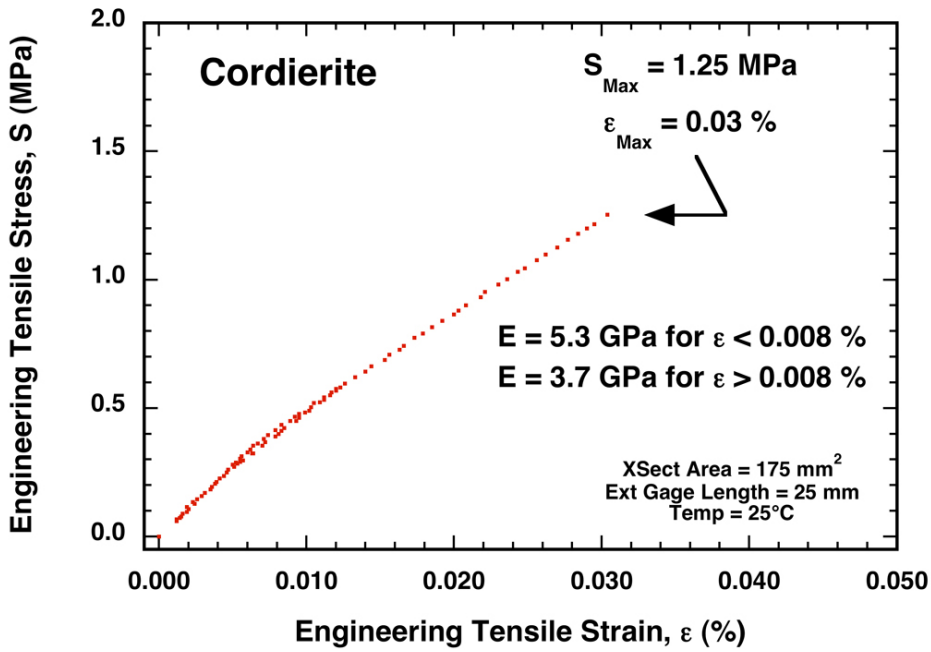

Figure 3. Representative tensile stress-strain curve measured with a cordierite DPF tensile specimen.

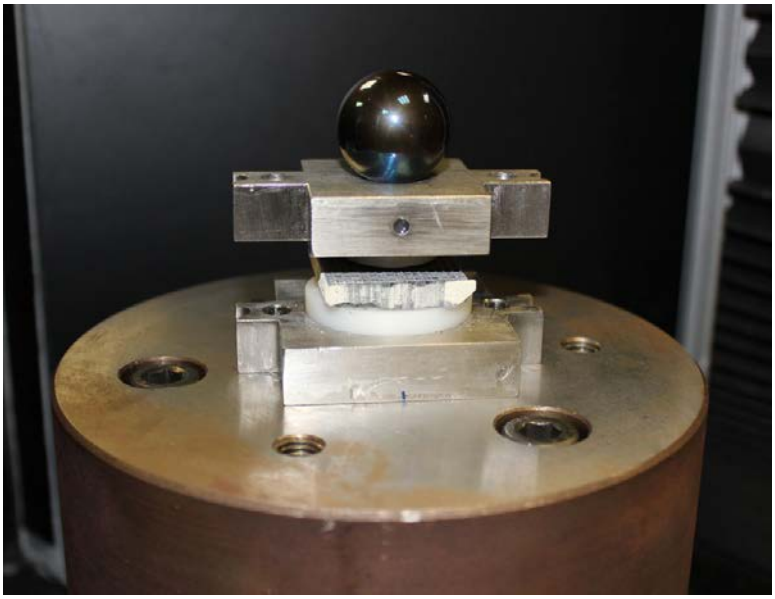

Figure 4. Biaxial flexure test setup for square SiC DPF test coupons.

Figure 5. GenSet with auxiliary fueling system and manifold panel.

A wideband lambda sensor, as shown in Figure 6, was added to monitor air/fuel ratio and oxygen content in the exhaust. A frequency signal conditioner was integrated into the data acquisition system to monitor generator performance, and help ensure repeatable operation. Efforts are nearly completed to allow 24 hour operation of the engine by means of interlocks and continuous signal analysis.

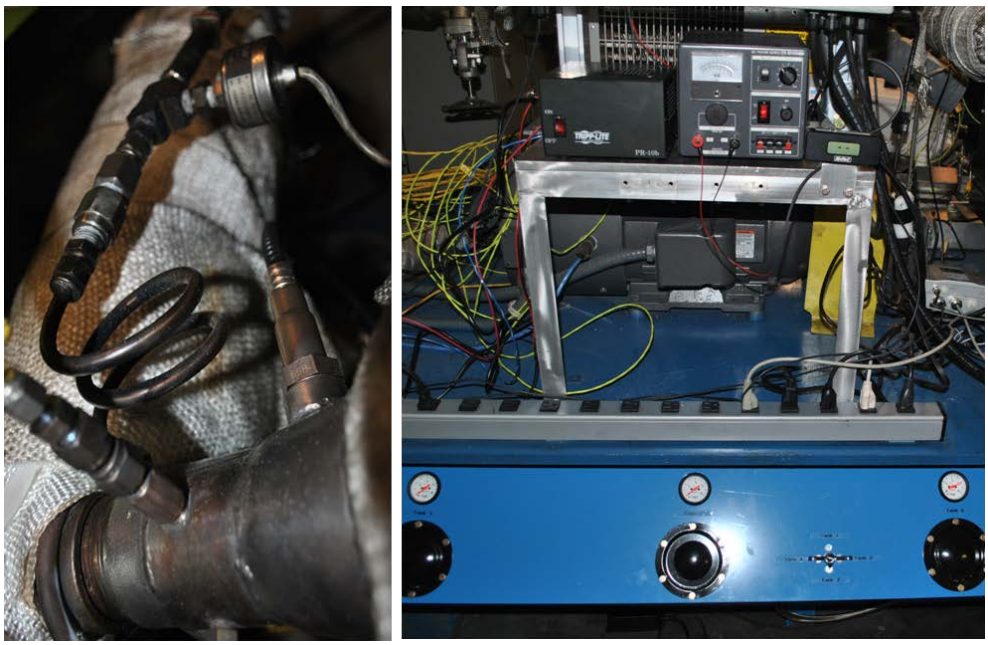

Figure 6. Wideband lambda sensor, pressure transducers and control hardware.

Status of FY2012 Milestones

1. Establish baseline mechanical testing of DPFs by measuring the elastic modulus and fracture strength of both the skin and interior of the DPF of both SiC (with 52 and 58% porosity) and cordierite (13 and 18 µm pore size) materials with at least 12 samples so as to determine fracture (Weibull) statistics. **(12/11)** *Completed.*
2. Age filter samples with Na and K doping in order to simulate long-term biodiesel exposure as dictated by the ASTM D6951 to 5 ppm and measure degradation using testing procedure developed in Milestone 1. **(9/12)** *On Schedule*

Communications/Visits/Travel

NREL's Aaron Williams visited ORNL on May 30 to discuss collaborative work involving DPFs and biofuels.

Problems Encountered

None

Publications/Presentations/Awards

None

References

None

Agreement 20091: Electrically Assisted DPF Material

M. J. Lance, J. E. Parks, A. A. Wereszczak, R. M. Connatser, V. Prikhodko, W. P. Partridge, E. E. Fox, and M. K. Ferber
Oak Ridge National Laboratory

Objective/Scope

In this CRADA project with General Motors (GM), two research objectives are being pursued:

1. Measure of substrate temperatures during DPF regeneration with optically based techniques that are not susceptible to conductive interferences that are problematic for common thermocouple technologies.
2. Analysis of diesel particulate filter (DPF) substrate materials to understand crack and failure mechanisms and resolve current differences in simulation and experimental results.

Technical Highlights

Thermomechanical modeling efforts continue to combine arbitrary estimates of the service conditions of a regenerating DPF with cordierite's measured mechanical properties to predict reliability and establish general rules of design. The properties of the DPF (elastic, thermoelastic, and strength), its dimensions, and temperature profile will be combined to identify whether or not failure initiation is likely.

Experiments on the GM 1.9-liter diesel engine platform to measure DPF substrate temperatures during regeneration with the blackbody radiation technique continued in Q3. In addition, data analysis of the blackbody spectra continued to derive temperature as a function of time and position in the DPF substrate. A complete set of temperature data was collected that contained temporal profiles of temperature as a function of position in the DPF substrate for various operating conditions. Results were compared for various particulate loadings including no loading to understand the effects of exothermic release of heat from the oxidizing particulate on substrate temperatures. While some measurements were made of DPF temperatures during fuel-based regeneration for the purpose of comparison, the majority of data collected was from the electrically assisted DPF regeneration technique of interest to GM.

An example of the temperature data collected during DPF regeneration is shown in Figure 1. Temperature data collected with both the blackbody radiation technique and standard thermocouples are shown. The blackbody radiation was collected by fiber optics inserted into the DPF flow channels with angled tips that enabled collection of light emitted from the substrate wall material. Thus, the blackbody radiation data represents the substrate temperature at the fiber optic probe location in the downstream flow channel of the DPF. In contrast, the thermocouple data represents the gas temperature at the thermocouple location (again, in the downstream flow channel of the DPF). Data is shown for two different particulate loadings where the loading in Fig. 1.b. is twice the amount for Fig. 1.a. A key finding from the data is that in no cases did we

observe the substrate temperatures exceeding the gas temperatures measured by the thermocouples. Thermocouples are prone to inaccuracies when conductive heat along the metal sheath artificially increases the reported temperature. The blackbody radiation technique gives a more representative measurement of the substrate temperatures on the downstream side of the DPF channel walls where the cleaned exhaust passes through. These substrate temperatures are more realistic data for predicting substrate durability with models.

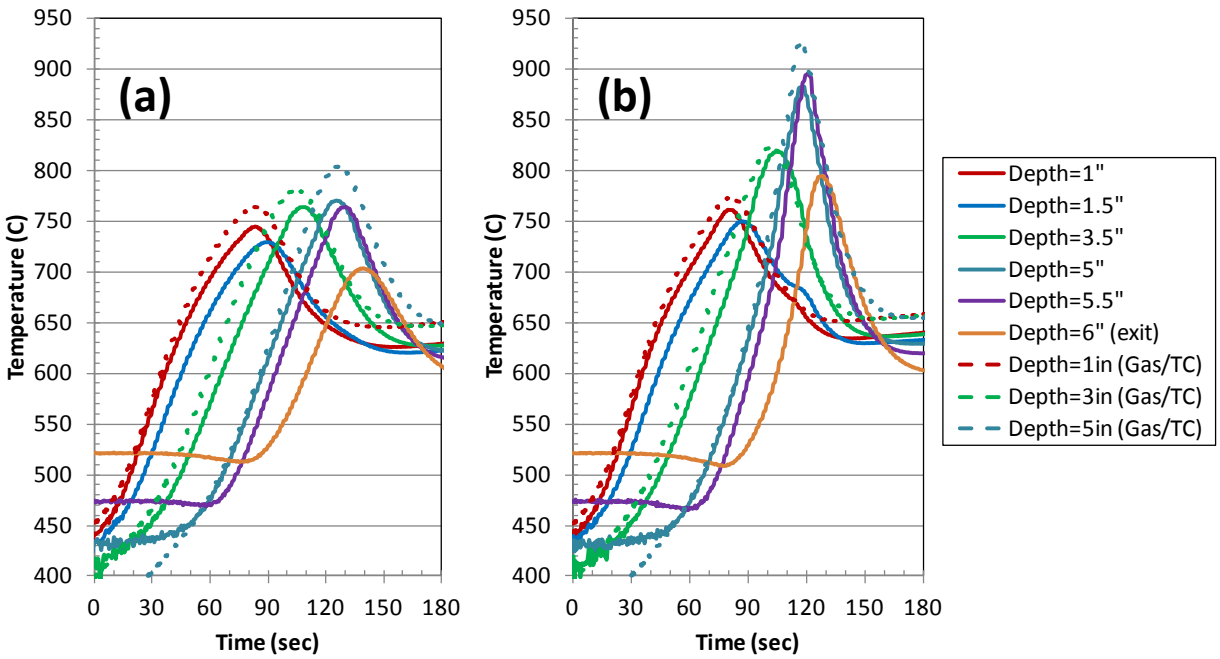

Figure 1. Temperature as a function of time during regeneration of the DPF with the electrically assisted technique. Data is shown for (a) 1x particulate loading and (b) 2x particulate loading at different depths into the exit flow channels of the DPF substrate (6" total length). Substrate temperatures measured with the fiber optic blackbody radiation technique are represented by the solid curves, and gas temperatures measured with thermocouples are represented by the dashed curves.

<u>Status of FY 2012 Milestones</u>

(1) Measurement of the wall temperature of the DPF at 8 different locations with a spatial resolution of 1 mm and temperature accuracy of +/- 10°C during regeneration at typical operating conditions (600-800°C) using a fiber optic technique. **(09/2012)** *Complete*

(2) Creation of DPF samples with a temperature exposure history equivalent to 15000 miles of operation on a light-duty vehicle for analysis by the MST team. **(09/2012)** *On Schedule*

(3) Measure retained strength of laboratory-exposed DPF specimens (provided by FEERC Team from Milestone 2) and extrapolate to the degradation expected from a lifetime of electrically-assisted regenerations (~700 cycles) in order to determine if the

improvement in engine efficiency from this technology is worth the potential decrease in substrate lifetime**. (09/2012)** *On Schedule*

Communications/Visits/Travel
None

Problems Encountered
None

Publications/Presentations/Awards
A. A. Wereszczak, E. E. Fox, M. J. Lance, and M. K. Ferber, "Failure Stress and Apparent Elastic Modulus of Diesel Particulate Filter Ceramics," was presented at the SAE 2012 World Congress, Detroit, MI, April 24-26, 2012. The paper will be published in the *SAE International Journal of Materials and Manufacturing*, 2012.

References
None

Agreement 9105: Characterization of Catalyst Microstructures

L.F. Allard, C.K. Narula, W.C. Bigelow, M.B. Katz, X. Pan, G. W. Graham, D.P. Nackashi and J. Damiano
Oak Ridge National Laboratory

Objective/Scope

The objective of the research is to understand fundamental processes in catalytic systems with applications to transportation technologies, such as those used for the treatment of NO_x emissions, and for the production of biomass-derived liquid fuels. The research heavily utilizes new capabilities and techniques for ultra-high resolution transmission electron microscopy with the HTML's aberration-corrected electron microscope (ACEM). The research is ultimately focused on understanding the effects of reaction conditions on the changes in morphology of heavy metal species on "real" catalyst support materials (e.g. oxides and carbon materials), and the understanding of the structures of model mono-, bi- and multi-metallic catalyst systems of known particle composition. A major thrust of these studies has been to develop methods of *in situ* microscopy at elevated temperatures and under controlled gas compositions. We have worked for some time with Protochips Inc. (Raleigh, NC), which provides a novel heating technology utilizing MEMS-based heating devices that we have shown to be stable enough to provide sub-Ångström imaging capabilities at high temperature in the ACEM. The devices have permitted the recent development of a closed-cell gas reaction holder that allows heating under controlled gas compositions up to a full atmosphere, with the ability to image atomic structure under these conditions. Methods using the new reactor (now called simply the "gas-cell holder") are currently being employed in a new study of "intelligent catalysts" for automotive emission control applications, based on the reported self-regenerative phenomenon of heavy metal species such as Pd and Rh in Ca- and La-based perovskite crystal structures. This work is being conducted in collaboration with Prof. Xiaoqing Pan of the University of Michigan, and his student Michael Katz and colleague George Graham, with further collaboration with Ford Research Laboratory colleague Dr. Andrew Drews.

Technical Progress

In situ gas-cell experiments designed to gain information on the behavior of catalytic species such as Pt and Rh in perovskite-based oxides such as calcium titanate (CTO), during oxidation and reduction cycles continued in the present quarter. These catalysts, previously termed "intelligent catalysts," are now being called "self-regenerative" catalysts, to more precisely describe their purported primary qualities. Specifically, we conducted experiments on Pt:CTO and Pt:BCO (barium cerate), in which the "as-prepared" materials (initially in an 'as-oxidized' state) were first reduced in our novel gas-cell specimen holder for the JEOL aberration-corrected electron microscope, then re-oxidized to observe how heavy metal species that are initially incorporated into the lattice of the oxide support particle form discrete catalytic particles on the surface of the support, then re-

dissolve into the lattice during the oxidation cycle. Two examples of results obtained on the above materials are given in the following.

Pt/CTO cycling: $CaTi_{0.95}Pt_{0.05}O_{3-\delta}$ powder was placed in the *in situ* holder and first examined in its as-prepared state, which comprised generally 50-200 nm single-crystal perovskite primary particles with a sparse dispersion of nascent Pt particles that formed during synthesis, shown in the high-angle annular dark-field (HAADF) image of Fig. 1a. During reduction in 5% H_2/Ar (or even vacuum), a plurality of small Pt clusters precipitated from the perovskite host (HAADF images of Figs. 1b,c). Actually, this reaction was nearly complete after only about 1 min of exposure to reaction conditions, with very little further Pt precipitation occurring at each reduction temperature shown. Without the capabilities of this *in situ* holder, reactions of this rate could not be easily examined. Though the position of the newly-formed Pt clusters relative to the perovskite particles is ambiguous due to the projective nature of STEM imaging, most are known to be within the bulk of the perovskite based on our previous work with model catalyst cross sections [1]. Oxidation at 800 °C in 20% O_2/N_2 followed, but was effective in inducing a number of only the smallest Pt clusters to re-dissolve into the perovskite host after an hour and longer (Fig. 2a,b), again in agreement with our previous findings. Because the specimen could be imaged at temperature in atmosphere, the stationary internal particles were easily distinguished from the mobile surface particles, which were in the process of coarsening over the duration of the experiment. Of special note is the considerable asymmetry with which the two halves of the reaction took place.

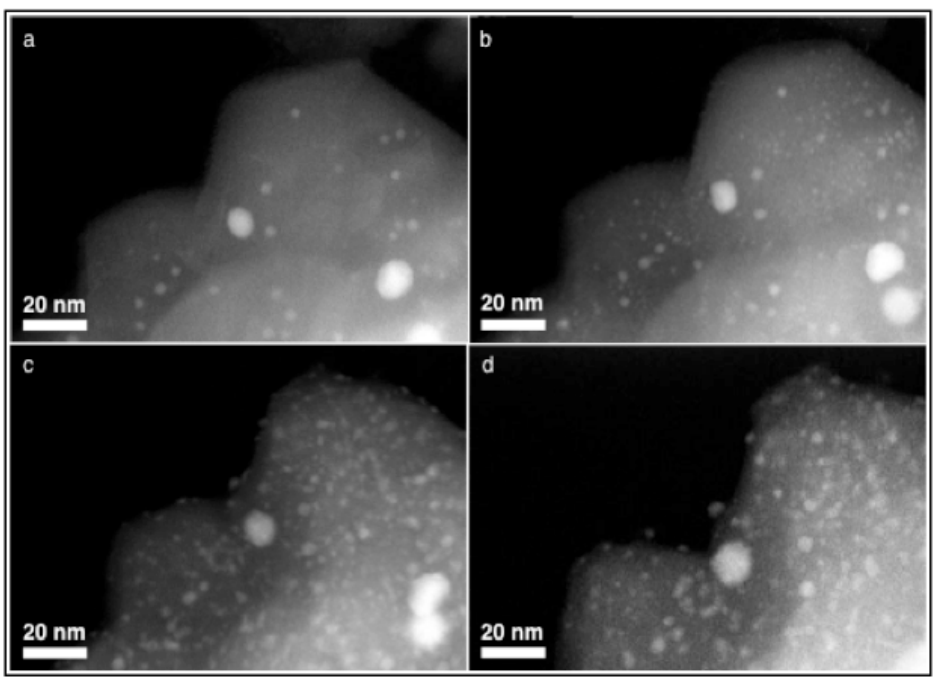

Fig 1. (a) A typical region of Pt:CTO powder as-prepared, showing nascent Pt particles; (b) the same region after 5 min. reduction at 600°C, (c) 5 min. at 800°C, and (d) 10 min. at 800°C (total reaction time 20 min.) showing extrusion of numerous Pt clusters to various extents.

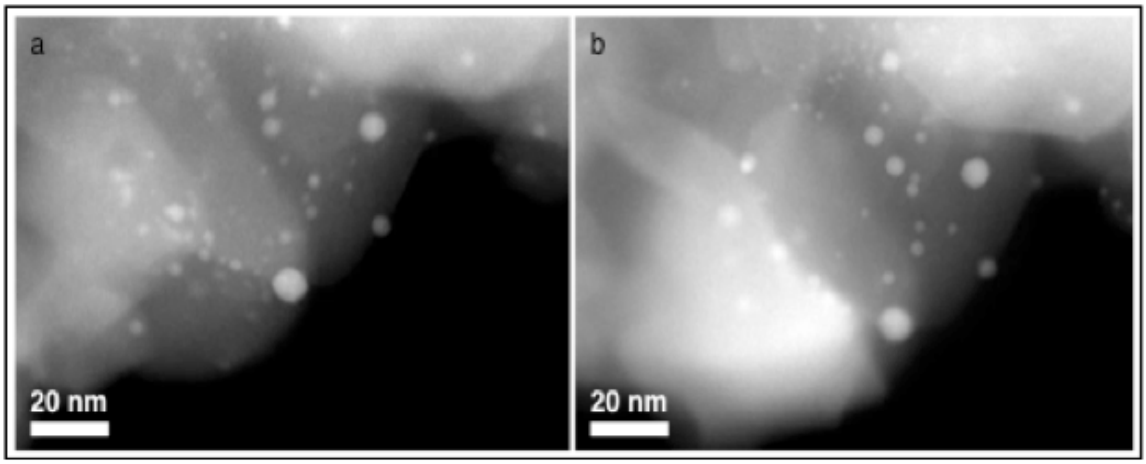

Fig 2. (a) A typical region of reduced Pt:CTO powder and (b) the same region after 100 min. of subsequent oxidation at 800°C. Only the smallest internal Pt clusters have dissolved. HAADF images.

Pt:BCO cycling: As-prepared (pre-oxidized) Pt:BCO material was imaged in several stages, as outlined:

- Stage 1: Load sample, view in vac at RT, image.
- Stage 2: Re-load cell, heat to 250°C, image.
- Stage 3: Add H_2, charge with 699.1 Torr, heat to 800°C for 1 minute and cool, then heat to 800°C for 9 minutes and cool, evacuate the cell, image in vacuum.
- Stage 4: Charge with 162.6 Torr O_2, heat to 800°C for 10 minutes and cool, image at pressure.
- Stage 5: Heat to 800°C for 50 minutes, cool, evacuate, image at pressure.
- Stage 6: Charge with 160 Torr H_2, heat to 800°C for 10 minutes and cool, evacuate, image at pressure.

Figure 3 shows a series of HAADF-BF image pairs illustrating the effects (as an example) of the behavior of a catalyst aggregate during stages 2, 3, 4 and 5 above. The BCO support in stage 2 initially appears as acicular crystals with little evidence of bright contrast from discrete Pt species, but after the reduction treatment at near atmospheric pressure (a capability unique to this “closed-cell” specimen holder geometry) and (a nominal) 800 °C for 10 minutes, the morphology showed a remarkable change, with the BCO material apparently strongly sintering, and Pt appearing as 10-20 nm discrete particles, at least some of which are on the surface as they appear in profile (stage 3). An oxidation treatment in stage 4, done at 800 °C and 162 Torr of O_2 for 10 min showed only a few changes in Pt particle morphology, such as the apparent disappearance of a particle marked A in the stage 3 image, which possibly coalesced to form the particle marked A’ in the stage 4 image, and the displacement of the particle marked B in the stage 3 image to a new position marked B’ in the stage 4 image.

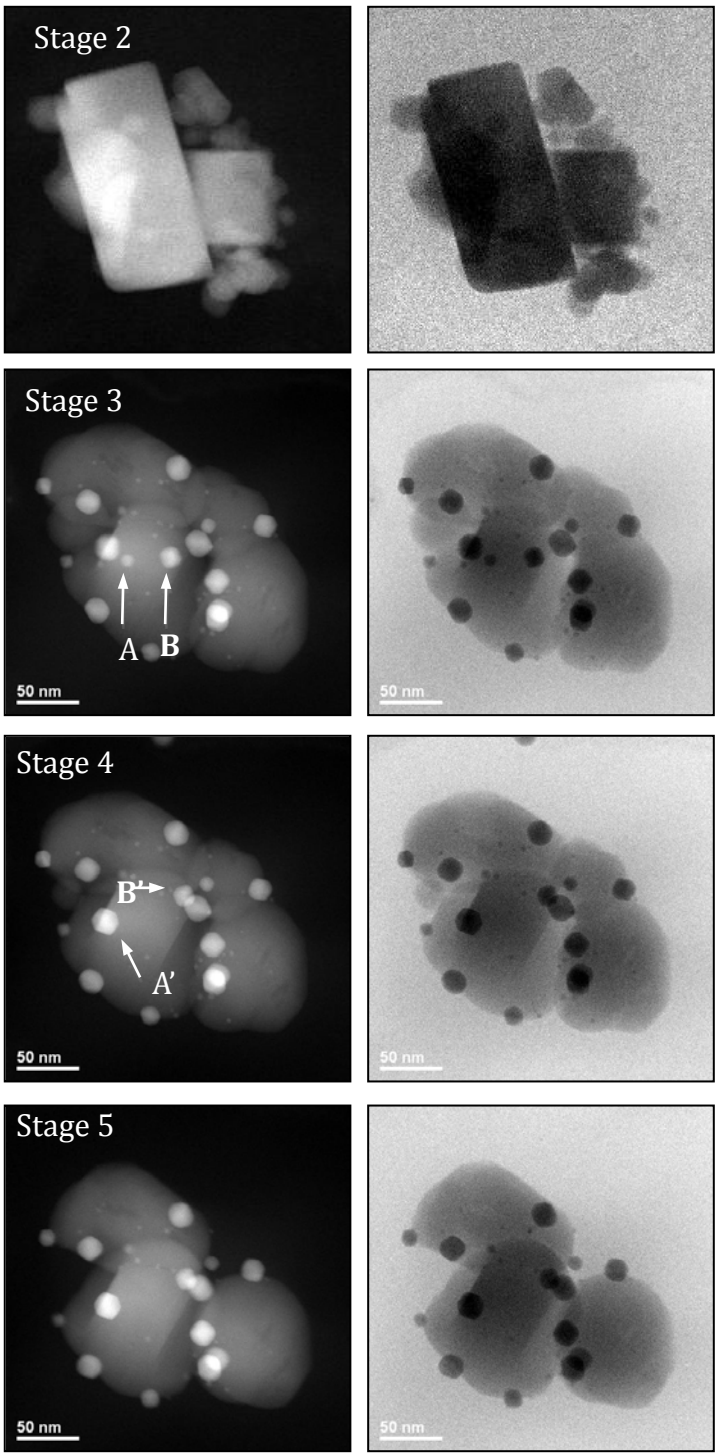

Fig. 3. HAADF-BF image pairs in a sequence of reaction stages showing redox effects on Pt:BCO catalyst material. See text for details.

Further oxidation for a total of 60 min at the same conditions yielded the image pair of stage 5, in which the major change in morphology was further sintering and coalescence of the BCO support material (thereby reducing the surface area

of support), and the obvious lack of any significant dissolution of the Pt particles into the support (but with most if not all of the Pt now present on the surface of the support.

These examples show the power of the in situ gas-reaction capability for observations of catalyst reactions. The above experiment are being analyzed in conjunction with a number of additional reaction runs to gain a better understanding of oxidation-reduction cycling on catalyst materials that may be candidates for self-regenerative applications.

References

1. Katz, M.B., *et al.*, *J. Amer. Chem. Soc.* **133** (2011) 18090.

Status of Milestones

On schedule

Communications/Visits/Travel

Larry Allard has developed a new association with BASF Co. (Islip, NJ) and, through an initial Work-for-Others (WFO) project funded by BASF has successfully completed analysis of an experimental catalyst material. BASF contact person was Dr. George Munzing. New work is presently being planned with other researchers at BASF.

Publications

"Novel MEMS-based Gas-Cell/Heating Specimen Holder Provides Advanced Imaging Capabilities for *In Situ* Reaction Studies," **L. F. Allard**, S. H. Overbury, W. C. Bigelow, M. B. Katz, D. P. Nackashi and J. Damiano; *Microscopy and Microanalysis*, In Press for July 2012**.**

Agreement 14957: High Temperature Thermoelectrics

A. A. Wereszczak and H. Wang
Oak Ridge National Laboratory
and
A. Thompson, R. McCarty, and J. Sharp
Marlow Industries, Inc.

Objective/Scope

Two-thirds of the chemical energy in automotive fuel is rejected to the atmosphere as waste heat. Thermomechanical stresses must be managed and TE material strength must be improved to fully exploit TE devices for waste heat recovery. Toward that, needed thermomechanical and thermophysical properties of candidate thermoelectric (TE) materials are measured in this project and then used with established probabilistic reliability and design models to optimally design automotive and heavy vehicle TE modules. Thermoelectric materials under candidacy for use in TE modules tend to be brittle, weak, and have a high coefficient of thermal expansion (CTE); therefore, they can be quite susceptible to mechanical failure when subjected to operational thermal gradients. A successfully designed TE module will be the result of the combination of temperature-dependent thermoelastic property and strength distribution data and the use of the method of probabilistic design developed for structural ceramics.

Technical Highlights

Mechanical Properties and Supportive Testing

An idle, low-temperature capable dual-rod dilatometer was worked on to resurrect its operation. Interest exists to measure the coefficient of thermal expansion (CTE) of thermoelectric device constituents down to at least -40°C, and this dilatometer was designed for that capability. It uses liquid helium as its coolant, and is able to also heat up to approximately 200°C. Various parts of its hardware were repaired and its stable operation was confirmed near the end of Q3 using a sapphire test coupon. The measurement of CTE of material constituents will commence in Q4.

The flexure strength as a function of temperature and the CTE of P-type skutterudites were measured in in Q3. These materials were co-fabricated by General Motors and Marlow.

Mechanical test methods are under development that will impose a graded strain on a thermoelectric device using biaxial flexure. This will allow the mimicking of thermal-gradient-induced strain on devices, and enable simplistic failure analysis study of the constituents in these devices.

Transport Property Measurements and IEA Activities

Two new skutterudites samples prepared by melt-spin and hot pressing were evaluated. Thermal diffusivity was measured using the Netzsch LFA457. The transport results were also compared with those from the University of Michigan (UofM). For system

calibration and comparison, a set of IEA-AMT samples from Marlow was sent to UofM. The n-type and p-type bismuth telluride materials had gone through two IEA-AMT international round-robin studies. The results will be compared to the Annex topical report.

Electrical resistivity and Temperature Coefficient of Resistance (TCR) of copper pastes were studied with coupons provided by Marlow. The copper was applied to alumina substrates and tested on a Signatone 4-point probe station. Electrical resistivity of different copper pastes and the TCR are important information for thermoelectric module design and have a direct impact on the device performance.

An initial study of efficiency testing was conducted. The focus was a survey of existing techniques, and analysis of the pros and cons of each technique. After discussion with Marlow Industries, a parallel approach using both the Harman technique and heat-flow efficiency test was adopted.

For the IEA-AMT efforts, the initial material, n-type PbTe, was determined to be too fragile for the round-robin study. Significant efforts were spent to machine specimens and despite those efforts, some samples shattered during preparation. Half-Heusler materials from GMZ Energy were then selected to replace the PbTe. The half-Heusler was prepared at GMZ and machined to specified dimension. During Q3 the specimens were measured by GMZ and Fraunhofer IPM in Germany. The specimens were received by the Shanghai Institute of Ceramics in late June. They will be circulated to the remaining round-robin participants in Q4 of FY12.

Status of FY 2012 Milestones

1. Measure mechanical, thermoelastic, and thermoelectric properties of Marlow-fabricated TE materials to enable reliable operation up to 500°C. **[Sep12]** *On schedule.*
2. Process and engineer sintered bulk polycrystalline Si to reduce its thermal conductivity to less than 10 W/mK. **[Sep12]** *Completed.*
3. Complete report of international round-robin test results on Marlow bismuth telluride to IEA-AMT and initiate a new high temperature thermoelectric round-robin measurements on PbTe or skutterudite ranging between 20 - 500°C. *On schedule.*

Communications/Visits/Travel:

The CRADA between Marlow Industries, Inc. and ORNL was extended to 31 March 2013 during the present reporting period. Numerous communications occurred between staff members at both Marlow and ORNL to administer that extension.

Wereszczak, Wang, and Allen Haynes visited Marlow Industry in Dallas on April 18-19 for a semi-annual CRADA project review meeting.

Wang attended the IEA-AMT Executive Committee meeting in Hamilton, ON, Canada on June 4-5. He also visited the CANMET facility during the meeting.

Problems Encountered
None

Publications/Presentations/Awards
H. Wang, et al., “Thermoelectric Round-robin Studies,” Technical Symposium of IEA-AMT, Hamilton ON, Canada June 4-5.

Wereszczak gave a presentation entitled "Thermoelectric Mechanical Reliability" at the 2012 Vehicle Technologies Annual Merit Review, Arlington, VA, on 15 May 2012.

References
None

Agreement 16308: MBD Thermoelectrics Theory and Structure

David J. Singh and David Parker
Oak Ridge National Laboratory

Objective/Scope

We will use modern science based materials design strategies to find ways to optimize existing thermoelectric materials and to discover new families of high performance thermoelectrics for waste heat recovery and vehicular cooling applications in vehicles. The emphasis will be on the thermoelectric figure of merit at temperatures relevant to waste heat recovery and vehicular cooling and on other properties important for applications, especially anisotropy, cost and mechanical properties.

Technical Highlights

Vehicular applications of thermoelectric materials for waste heat recovery, as well as passenger cabin heating and cooling (needed for the performance of hybrid electric vehicles), necessitate the study and identification of high performance materials. These materials must have the contradictory properties of good electrical conductivity and high Seebeck coefficient, and low thermal conductivity but high electrical conductivity.

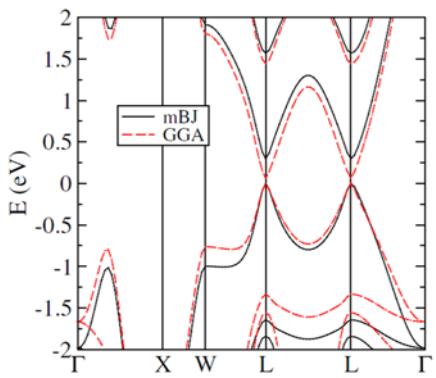

Figure 1: Band structure of PbSe, comparing standard density functional calculations and calculations with the newly developed mBJ functional.

We predicted in 2010 [1] that hole-doped PbSe could be a high performance thermoelectric material if properly optimized, with ZT values as high as 2 at 1000 K, in contrast to then-existing knowledge. This prediction has been essentially confirmed by work from the group of Z.F. Ren [2] who find a ZT value of 1.7 at 875 K in hole-doped PbSe. This is a major finding given that ZT=2.0 forms a "practicality threshold" for exhaust waste heat recovery and the DOE goal of a 10% fuel economy increase [3] from exhaust waste heat recovery. We also considered electron-doped PbSe and found that ZT values of 0.9 were possible. The main reason that we identified for the difference between the hole-doped and electron-doped predictions were the presence of a heavy band below the valence band maximum, and the rather small band gap (0.065eV) found in our 2010 first principles calculations. More recently a new functional called "mBJ" has become available and we have been testing it for thermoelectrics. This functional gives improved band gaps and so we are now using this new technology in our calculations. Recent experimental work by the group of Z.F. Ren [4] finds better n-type ZT values of 1.3 for PbSe. We have therefore revisited [5] electron-doped PbSe with this new method [6]). The experimental band gap of PbSe is 0.27 eV [7] and our revised calculations find a band gap of 0.30 eV, in excellent agreement with the experimental value. The revised (mBJ) and original (GGA) band structures are presented in Figure 1. The band gap revision is crucial for

performance (i.e., ZT) predictions as a small band gap can lead to bipolar conduction which is generally destructive to thermoelectric performance.

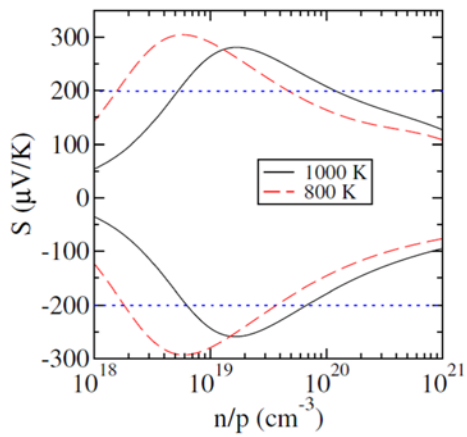

Figure 2: Calculated thermopower of p-type and n-type PbSe as a function of doping level as with use of the mBJ functional.

With this new electronic structure we find that n-type PbSe can show Seebeck coefficients as high in magnitude as 250 μV/K at 1000 K and nearly 300 μV/K at 800 K. These values are substantially larger than the 160 μV/K maximum Seebeck coefficient magnitude for n-type PbSe found in the earlier work and mean that, like p-type PbSe, n-type PbSe can also be a high performance material. Based on these results, it seems that the best reported n-type materials are not fully optimized yet, and that significant performance increases from the ZT=1.3 value found experimentally may be possible. Such a combination of good high temperature n-type and p-type performance will be highly beneficial to the waste heat recovery efforts since such applications necessarily require both n-type and p-type materials to function. An additional benefit is that it is important for the p and n-type legs in a thermoelectric module to be well matched in mechanical properties such as thermal expansion, so that finding high thermoelectric performance for both n-type and p-type doping <u>in the same material</u> is a substantial development. We note also that PbSe is a cubic and therefore isotropic material, a significant advantage for applications.

We note that while our prediction that the performance of n-type PbSe can improved by optimization of the carrier concentration remains to be proven, we do find good agreement with existing experiments at the doping levels where those experiments were performance. To illustrate this, we present in Figure 3 a comparison of our calculated thermopower and the experimental data (note that we have assumed a band gap of 0.38 eV for this calculation as there is evidence that the band gap of PbSe increases with temperature). We find excellent agreement. As with our original PbSe work, this shows that our theoretical calculations have accuracy sufficient to have predictive power – a fact of vital importance in the search for high performance thermoelectric materials.

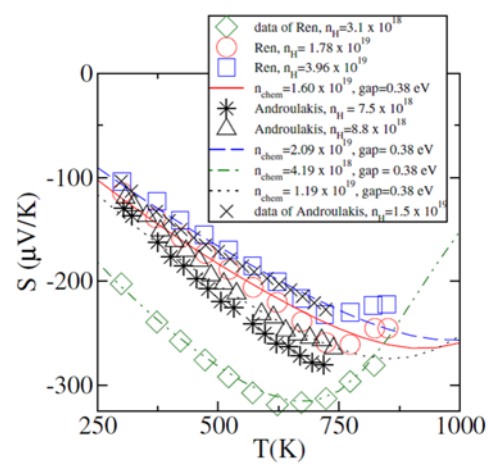

Figure 3: Calculated thermopower of n-type PbSe compared with experimental data of Ren et al. [4] and Androulakis et al. [8].

Status of FY 2012 Milestones

We are making progress towards our milestone of successfully predicting new thermoelectric compositions. We plan to explore the potential thermoelectric performance of the copper oxide materials CuBiSeO and CuBiSO, both composed of inexpensive and abundant elements, and to continue investigation of chalcogenides.

Problems Encountered

No significant problems encountered this quarter.

Publications/Presentations/Awards

1. D. Parker, D.J. Singh, Q. Zhang and Z. Ren "Thermoelectric properties of n-type PbSe revisited," J. Appl. Phys. **111**, 123701 (2012).

References

1. D. Parker and D.J. Singh, "High-temperature thermoelectric performance of heavily doped PbSe," Phys. Rev. B **82**, 035204 (2010).
2. Q. Zhang, F. Cao, W. Liu, K. Lukas, B. Yu, S. Chen, C. Opeil, D. Broido, G. Chen, and Z. Ren, "Heavy Doping and Band Engineering by Potassium to Improve the Thermoelectric Figure of Merit in p-Type PbTe, PbSe, and $PbTe_{1-y}Se_{y,}$" J. Am. Chem. Soc. **134**, 10031 (2012).
3. Vehicle Technologies Multiyear Program Plan 2010-2015, Section 2.3.2, "Solid State Energy Conversion."
4. Q. Zhang, H. Wang, W. Liu, H. Wang, B. Yu, Q. Zhang, Z. Tian, G. Ni, S. Lee, K. Esfarjani, G. Chen and Z. Ren, "Enhancement of thermoelectric figure-of-merit by resonant states of aluminum doping in lead selenide," Energy and Env. Science **5**, 5246 (2012).
5. D. Parker, D. J. Singh, Q. Zhang, and Z. Ren, "Thermoelectric properties of n-type PbSe revisited," J. Appl. Phys. **111**, 123701 (2012).
6. F. Tran and P. Blaha, "Accurate Band Gaps of Semiconductors and Insulators with a Semilocal Exchange-Correlation Potential," Phys. Rev. Lett. **102**, 226401 (2009).
7. Springer Materials Landolt-Bornstein database, available online at http://www.springer.com/librarians/e-content/springermaterials?SGWID=0-171102-0-0-0.
8. J. Androulakis, Y. Lee, I. Todorov, D.-Y. Chung and M. Kanatzidis, "High-temperature thermoelectric properties of n-type PbSe doped with Ga, In, and Pb," Phys. Rev. B **83**, 195209 (2011).